Discovery of embryonically derived bipotent endothelial-macrophage progenitor cells in postnatal aorta

Anna E. Williamson PhD[1,2†], Sanuri Liyanage PhD[1,2†], Mohammadhossein Hassanshahi PhD[1,2], Malathi S.I. Dona PhD[3], Deborah Toledo-Flores MBBS PhD[1], Dang X.A. Tran BSc[1], Catherine Dimasi BSc[1], Nisha Schwarz PhD[1], Sanuja Fernando PhD[1,2], Thalia Salagaras BSc[1], Aaron Long MBBS[1,4], Jan Kazenwadel PhD[5], Natasha L. Harvey PhD[2,5], Grant R. Drummond PhD[6], Antony Vinh PhD[6], Vashe Chandrakanthan PhD[7], Ashish Misra PhD[8], Zoltan Neufeld PhD[9], Joanne T.M. Tan PhD[1,2], Luciano Martelotto PhD[10], Jose M. Polo PhD[10], Claudine S. Bonder PhD[5], Alexander R. Pinto PhD[3,6], Shiwani Sharma PhD[1,11], Stephen J. Nicholls MBBS PhD[12], Christina A. Bursill PhD[1,2], Peter J. Psaltis MBBS PhD[1,2,4*]

[1] Vascular Research Centre, Heart and Vascular Program, Lifelong Health Theme, South Australian Health and Medical Research Institute, Adelaide, South Australia, 5000 Australia

[2] Adelaide Medical School, Faculty of Health and Medical Sciences, The University of Adelaide, Adelaide, South Australia, 5000, Australia

[3] Cardiac Cellular Systems Laboratory, Baker Heart and Diabetes Institute, Melbourne, Victoria, 3004, Australia.

[4] Department of Cardiology, Royal Adelaide Hospital, Central Adelaide Local Health Network, Adelaide, South Australia, 5000, Australia

[5] Centre for Cancer Biology, University of South Australia and SA Pathology, Adelaide, South Australia, 5000, Australia

[6] Department of Microbiology, Anatomy, Physiology and Pharmacology and Centre for Cardiovascular Biology and Disease Research, School of Agriculture, Biomedicine and Environment, La Trobe University, Bundoora, Victoria, 3086, Australia.

[7] School of Medical Sciences, University of New South Wales, Sydney, New South Wales, 2052, Australia

[8] Faculty of Medicine and Health, University of Sydney and Heart Research Institute, Newtown, New South Wales, 2042, Australia

[9] School of Mathematics and Physics, The University of Queensland, Brisbane, Queensland, 4072, Australia

[10] Adelaide Centre for Epigenetics and the South Australian Immunogenomics Cancer Institute, Faculty of Health and Medical Sciences, The University of Adelaide, Adelaide, SA 5000, Australia

[11] Flinders Medical Research Institute, College of Medicine and Public Health, Flinders University, Bedford Park, SA 5042, Australia

[12] Monash Cardiovascular Research Centre, Monash University, Clayton, Melbourne, Victoria, 3800, Australia

† equal contribution; * corresponding author

Address for Correspondence:

Peter J. Psaltis, MBBS PhD

Vascular Research Centre, Lifelong Health Theme, Level 6

South Australian Health and Medical Research Institute

PO Box 11060, Adelaide, SA, 5001, Australia.

Tel: +61 8 8128 4534; Fax: +61 8 8362 2724; Email: peter.psaltis@sahmri.com

ABSTRACT

Background: Yolk sac (YS) progenitors are a source of macrophages and endothelial cells in some tissues that are thought to be maintained postnatally by self-renewal in their differentiated states. How this is achieved remains poorly understood.

Methods and Results: Single-cell digests from mouse aortas selectively formed macrophage colony-forming units (CFU-M) in methylcellulose, which self-renewed in secondary cultures from single cells. CFU-M comprised a homogeneous population of $Lin^{-}CD45^{+/Lo}CD11b^{-}F4/80^{-}Sca\text{-}1^{+}c\text{-}Kit^{+}$ progenitor cells that co-expressed fractalkine receptor (CX_3CR1) and colony stimulating factor-1 receptor (CSF1R). These progenitors displayed high proliferative activity from adult aorta even at steady state. *Flt3*^{Cre} lineage mapping revealed their independence from $Flt3^{+}$ bone marrow hematopoietic progenitor cells. They were especially abundant in neonatal aorta, with subsequent age-related decline, suggesting prenatal seeding, which was confirmed by finding their emergence in YS after embryonic day (E) 7.5 and from aorta-gonad-mesonephros by E10.5. Inducible fate-mapping using *Csf1r*$^{Mer\text{-}iCre\text{-}Mer}$ and *Cx3cr1*$^{YFP\text{-}creER}$ mice established that these progenitors originate from an E8.5 $CSF1R^{+}$ and E8.5-9.5 CX_3CR1^{+} source, together with macrophages and endothelial cells in the aortic wall. Complementary differentiation studies revealed aortic progenitors to be vasculogenic and bipotent for macrophages and endothelium, contributing to adventitial neovascularization in aortic ring assays and forming perfused blood vessels and macrophages after transfer into ischemic hindlimb. Single-cell RNA sequencing showed their relatively homogeneous myelopoietic and angiogenic gene expression profile without expression of mature myeloid or endothelial genes. Finally, we found that aortic progenitors also express angiotensin converting enzyme (ACE) and angiotensin II receptor, AGTR2, and established regulatory roles for angiotensin II, which augmented their proliferative, self-renewal and differentiation properties *in vitro* and expansion in aorta *in vivo*.

Conclusion: Our discovery of aortic endothelial-macrophage progenitors adds to the recognized fate of YS progenitors in postnatal tissues. These bipotent cells may help explain the local renewal of YS-derived tissue-resident macrophages and endothelial cells after birth.

KEYWORDS

Angiotensin II, CSF1R, CX_3CR1, Endothelial cell, Hemangioblast, Lineage mapping, Macrophage, Progenitor cell, Vasculogenesis, Yolk sac.

INTRODUCTION

Among diverse roles, macrophages are integral to development of blood and lymphatic vessels during normal organogenesis and responses to tissue injury, ischemia and other diseases [1-4]. They proliferate and assemble around neovessels, producing angiogenic factors and supporting endothelial anastomoses and vascular remodeling [2]. In return, endothelial cells help regulate the self-renewal of hematopoietic stem cells (HSCs) and their differentiation into macrophages [5]. Understanding how macrophage-endothelial interactions arise is important to target inflammation and neovascularization in different pathophysiological conditions.

Historically, circulating monocytes were thought to be the source of tissue macrophages [6]. Monocytes derive from definitive hematopoiesis, which originates embryonically with emergence of HSC clusters from the endothelium of the aorta-gonad-mesonephros (AGM) at around embryonic day (E) 10.5 in mice [7-9]. These HSCs seed fetal liver before colonizing bone marrow (BM) perinatally, the main hematopoietic organ after birth. Numerous studies have now established that HSC-monocyte ancestry does not account for all tissue macrophages [10-16]. During embryogenesis, extra-embryonic yolk sac (YS) is the first site to produce macrophages via distinct developmental programs. This begins with primitive macrophage precursors in YS blood islands between E7.0 and E8.25 [17, 18], followed by erythromyeloid progenitors (EMPs) which bud from specialized YS hemogenic endothelium [19]. From E7.5, c-Kit^{+}CSF1R^{+} EMPs produce erythrocytes, megakaryocytes and YS macrophages in a process that is independent of the transcription factor, Myb [11, 16, 20]. This does not involve monocyte intermediates but rather sequential differentiation into CX$_3$CR1^{+} pre-macrophages and mature F4/80^{Hi} macrophages [17, 21-23]. Macrophage progenitors, in both multipotent EMP and pre-macrophage stages, expand in YS and circulate to embryonic

tissues to complete their maturation [24]. This migration peaks around E10.5 and is mostly complete by E12.5. From E8.5, Myb^{+}c-Kit^{+}CSF1R^{Lo} EMPs also differentiate into YS macrophages and traffic to liver, where they expand and generate lineage-specific hematopoietic progenitors and fetal blood cells, including monocytes [23, 25]. Long-lived populations of embryonically derived macrophages persist in adult tissues, including brain, skin, liver, heart, lung and aortic adventitia [10-16, 26]. These are maintained independently of BM hematopoiesis through local proliferation and seemingly, by self-renewal [27].

Recent studies indicate that YS EMPs also contribute endothelial cells to the blood and lymphatic vessels of some organs [4, 28]. Although disputed [29], the possibility that EMPs produce both hematopoietic and endothelial cells is intriguing, especially given long-standing speculation around the embryonic existence of mesoderm-derived hemangioblasts [30]. While hemangioblasts have been shown to emerge during hemato-endothelial differentiation of pluripotent stem cells *in vitro* [31, 32], their presence in postnatal tissues remains unproven [33]. Here, we identify clonogenic endothelial-macrophage (EndoMac) progenitor cells in postnatal aorta, that are embryonically derived from YS EMPs and are seeded around E10.5 of gestation. These highly proliferative progenitors are independent of BM hematopoiesis and are a local source of macrophage and endothelial renewal and expansion during adventitial neovascularization.

RESULTS

c-Kit and CX$_3$CR1 identify CFU-M progenitors in postnatal aorta

Previously, we identified that the adventitia of mouse arteries contains cells with hematopoietic potential that selectively produce macrophage colony-forming units (CFU-M) in methylcellulose [34, 35]. To establish the true nature of these CFU-M forming cells, we began

by culturing aortic digests from 12-week-old (w) C57BL/6J mice in methylcellulose (MethoCult GF M3434, StemCell Technologies) for 14 days (d). This generated 17.0±12.0 CFU-M/10^5 cells (n=10), with colonies further classified based on size as ~77% small (~30-100 cells), ~23% medium (~100-1000 cells) and <1% large (>1000 cells) (**Figure 1A**). Data from other studies have been interpreted to support the self-renewal of mature macrophages in postnatal aorta [15, 36]. We therefore investigated whether adult aortic CFU-M can renew *in vitro*. CFU-M were isolated and disaggregated, with their content replated in single-cell secondary (2°) cultures for another 14 d in methylcellulose. Daily inspection revealed that single cells from small CFU-M gave rise to 2° clusters (<30 cells), whereas those from medium CFU-M generated small 2° colonies (**Figure 1B**), with renewal frequency of 1 new colony produced per ~15 cells. We observed no further colony formation in tertiary cultures, indicating that the renewal ability of CFU-M from adult C57BL/6J aortas is finite.

Having established that medium CFU-M form 2° colonies from a single-cell source, we used flow cytometry to examine their composition. This revealed a population in both 1° and 2° CFU-M that was predominantly negative for lineage (Lin) and monocyte/macrophage markers (CD11b, F4/80), but positive for CD45, Sca-1, c-Kit, CX_3CR1 and CSF1R (**Figure 1C, D** and **Supplemental Figure S1A**). In contrast, large CFU-M which were only rarely produced from adult aorta, contained 32.0±8.8% $CD45^+CD11b^+F4/80^+$ macrophages (n=6). These were located on the outer perimeter of large colonies, while the inner core was made up of $Lin^-CD45^+CD11b^-F4/80^-Sca\text{-}1^+c\text{-}Kit^+$ progenitors. Medium CFU-M also expressed the hematopoietic progenitor and EMP markers, CD34, CD16/32, CD93 (AA4.1) and CD43 [37], but not CD41 (very early-stage hematopoiesis) or Flt3 (CD135) (definitive hematopoiesis) (**Supplemental Figure S1B**). The stem cell marker, c-Myc, which regulates self-renewal was expressed in 15.0±5.4% of permeabilized cells, while Sox2, Nanog and Oct4 which are also

associated with pluripotency, were very lowly expressed. Other mature myeloid markers were negative (<1%) (CD64, CD86, MerTK) or lowly expressed (CD24, MHC II, CCR2, Ly6C, Gr1, LYVE-1). Medium CFU-M were also negative for the erythroid marker, TER-119, and endothelial marker, CDH5 (CD144), with <5% surface expression of VEGFR2 and TIE2; however, they did express CD31, which is also found on myeloid progenitors [17] (**Supplemental Figure S1B**). Immunofluorescence labeling and confocal microscopy also showed that progenitors in aortic CFU-M were proliferating ($Ki67^+$) and homogeneously c-Kit^+, but were negative for the macrophage marker, CD68, and endothelial marker, Endomucin (EMCN) (**Supplemental Figure S2A**).

Importantly, we identified $Lin^-CD45^{+/Lo}CD11b^-F4/80^-Sca\text{-}1^+c\text{-}Kit^+$ progenitors in 12 w C57BL/6J aorta *in vivo* (0.40±0.31% or 3,308±2,967 cells per aorta, n=4), resembling the surface phenotype of CFU-M (**Figure 1E** and **Supplemental Figure S1A**). Bromodeoxyuridine (BrdU) uptake 24 h after administration revealed that ~43% of these progenitors were in S-phase of cell cycle, compared to ~13% of macrophages in donor-matched aortas (**Figure 1F**). We also used fluorescence activated cell sorting (FACS) of aortic digests from C57BL/6J mice to isolate $CD45^+CD11b^-F4/80^-Sca\text{-}1^+c\text{-}Kit^+$ progenitors and confirmed their ability to form CFU-M (**Supplemental Figure S2B-D**). These colonies had similar surface marker expression as the medium CFU-M grown from unfractionated aortic cells (**Supplemental Figure S2E**). In contrast, no colonies grew from isolated $CD45^+CD11b^+F4/80^+$ macrophages.

Fractalkine receptor, CX_3CR1, has been used to characterize tissue-resident macrophages, including those in adventitia, and to trace their embryonic origins [12, 14, 15]. As CFU-M progenitors expressed CX_3CR1, we studied *Cx3cr1*$^{GFP/+}$ mice which express green fluorescent

protein (GFP) under control of the *Cx3cr1* locus [38]. CFU-M from *Cx3cr1*$^{GFP/+}$ aortas were GFP^{+} under fluorescence microscopy and flow cytometry (**Supplemental Figure S3A**). Whereas other studies have focused on CX_3CR1 expression by aortic macrophages [15], we also identified CX_3CR1^{+}c-Kit^{+} progenitors in aortic adventitia (**Figure 1G**) and determined by flow cytometry that they accounted for 18.9±4.7% of CX_3CR1^{+} cells in the aortic wall (n=6) (**Supplemental Figure S3B, C**). FACS isolation of aortic cells from *Cx3cr1*$^{GFP/+}$ mice showed that CFU-M forming capacity was restricted to GFP^{+} (especially GFP^{Bright}) cells (**Supplemental Figure S3D**), and specifically GFP^{+}CD11b^{-}F4/80^{-} progenitors, not GFP^{+} macrophages (**Figure 1H** and **Supplemental Figure S3E, F**).

As evidence of the functional importance of CX_3CR1, addition of its ligand, CX_3CL1, resulted in 1.6-fold higher CFU-M yield from aortic cells (**Figure 1I**), similar to the effect of macrophage colony-stimulating factor (M-CSF), the ligand for CSF1R (**Figure 1J**). We also compared *Cx3cr1*$^{GFP/+}$ mice to *Cx3cr1*$^{GFP/GFP}$ littermates, that lack both functional *Cx3cr1* alleles. *Cx3cr1*$^{GFP/GFP}$ aortas had lower CFU-M yield (**Figure 1K**) and contained ~60% fewer progenitors by flow cytometry (**Figure 1L**). Therefore CX_3CR1 is both a marker of CFU-M progenitors and promotes their clonogenicity and prevalence in aorta.

Aortic CFU-M progenitors are independent of bone marrow hematopoietic progenitors

C-C chemokine receptor 2 (CCR2), the cognate receptor for C-C chemokine ligand 2 (CCL2), has been used to differentiate between monocyte-derived (CCR2^{+}) and locally maintained, embryonically derived (CCR2^{-}) macrophages in some tissues [39]. Unlike CX_3CR1, CCR2 was lowly expressed on aortic CFU-M progenitors (**Supplemental Figure S4A**). Aortic cells from *Ccr2*$^{-/-}$ mice formed more CFU-M than wildtype littermates, with a higher percentage of progenitors, despite fewer circulating monocytes (**Supplemental Figure S4B-D**). Similarly,

when clodronate liposomes were used to deplete blood monocytes, we observed a significant increase in aortic CFU-M formation (**Supplemental Figure S4E-G**). Both these results suggest that the size of the aortic progenitor population is not dependent on circulating monocytes.

This led us to examine the relationship between CFU-M progenitors and BM hematopoiesis by using *Flt3*^{Cre} x *Rosa*$^{mT/mG}$ mice. BM hematopoietic progenitors transiently upregulate the receptor tyrosine kinase Flt3 during hematopoietic differentiation [40]. In *Flt3*^{Cre} x *Rosa*$^{mT/mG}$ mice cells that originate from BM hematopoietic progenitors express GFP (Flt3-Cre^{+}), while those that do not are GFP^{-} and express tdTomato (tdTom) (Flt3-Cre^{-}). Adult aortic CFU-M from *Flt3*^{Cre} x *Rosa*$^{mT/mG}$ mice were ~95% Flt3-Cre^{-}, while BM produced a mixture of CFU-M and non-macrophage colonies that were ~90% Flt3-Cre^{+} (**Figure 2A, B**). Similarly, peripheral blood monocytes were predominantly Flt3-Cre^{+}, whereas aorta contained Lin^{-} CD45$^{+/Lo}$CD11b^{-}F4/80^{-}Sca-1^{+}c-Kit^{+} progenitors that were mostly Flt3-Cre^{-} (**Figure 2C**). In keeping with previous studies [15, 36], aorta contained a mixture of Flt3-Cre^{+} (~85%) and Flt3-Cre^{-} (~15%) macrophages (**Supplemental Figure S4H**). For reference, macrophages in BM and spleen were >95% Flt3-Cre^{+} and brain microglia ~94% Flt3-Cre^{-}. Therefore, aortic CFU-M progenitors are unlikely to be derived from BM hematopoietic progenitors.

Aortic CFU-M progenitors are seeded embryonically

To further elucidate the origins of aortic CFU-M progenitors, we performed age profiling after birth. Aortic CFU-M yield was ~10-fold higher from P1 (postnatal day 1) than 3 w and 12 w mice, and lowest from 52 w mice (**Figure 2D**). P1 aortas produced more large and medium colonies, with the latter showing greater ability to form 2° colonies after single cell replating than was the case from older mice (**Supplemental Figure S4I, J**). Flow cytometry

supported the higher abundance of progenitors in P1 aorta and their declining prevalence as mice age (**Figure 2E**).

As aortic CFU-M progenitors are present at birth, we examined their emergence during embryonic development. CFU-M grew from digests of YS from E7.5, with their yield peaking at E9.5 (**Figure 2F** and **Supplemental Figure S4K**). 2° renewal capacity was 100% with one new colony formed for each cell plated from medium CFU-M from E9.5 YS (**Supplemental Figure S4J**). Although CFU-M were rare from digests of whole embryo between E7.5 and E9.5, they were more prevalent from AGM from E10.5 onwards (**Figure 2F**). Coinciding with the emergence of definitive HSCs from dorsal aorta at ~E10.5-11.5 [9], we also observed non-macrophage colonies (G, granulocyte; GM, granulocyte-macrophage; GEMM, granulocyte-erythrocyte-monocyte-megakaryocyte; BFU-E, burst-forming units-erythroid) from AGM during this gestational window (**Supplemental Figure S4L**). However, unlike CFU-M these disappeared by E12.5. Colony growth from liver increased between E10.5 and E11.5 and consisted mostly of non-macrophage colonies through to E15.5, consistent with seeding of HSCs and multipotent progenitors from AGM and YS [23, 25] (**Supplemental Figure S4M**).

We next investigated which cells in early YS are responsible for producing CFU-M. Using *Cx3cr1*$^{GFP/+}$ embryos, three populations were FACS isolated from E9.5 YS: 1) CX_3CR1/GFP^+c-Kit^+CD45^+, 2) CX_3CR1/GFP^-c-Kit^+CD45^+ and 3) CX_3CR1/GFP^+c-Kit^- $CD45^+$ cells (**Supplemental Figure S5A**). CFU-M were selectively produced by the CX_3CR1/GFP^+c-Kit^+CD45^+ fraction (**Figure 2G** and **Supplemental Figure S5B**). These CFU-M expressed surface markers consistent with those of CFU-M from adult aorta (**Figure S5C**) and were able to renew from a single-cell source with 78% (7 out of 9 replicate wells)

and 14% (1 out of 7) efficiency after 2º and 3º replating, respectively. In contrast, CX_3CR1/GFP^-c-Kit^+CD45^+ progenitors produced mostly non-macrophage colonies, while no colonies grew from CX_3CR1/GFP^+c-Kit^-CD45^+ cells (**Figure 2G** and **Supplemental Figure S5B**). We also observed the presence of CX_3CR1/GFP^+c-Kit^+CD45^+ progenitors in YS from E8.5 and AGM from E10.5, in keeping with CFU-M growth (**Figure 2H, I** and **Supplemental Figure S5D, E**). Finally, using confocal microscopy, we identified CX_3CR1/GFP^+c-Kit^+ progenitors in aortic adventitia at E12.5 and E15.5 (i.e., after disappearance of definitive HSCs from AGM) (**Figure 2J**).

Aortic CFU-M progenitors originate from CX_3CR1^+ and $CSF1R^+$ embryonic progenitors

Murine aortic adventitia has been shown to contain locally maintained macrophages derived from CX_3CR1^+ and $CSF1R^+$ YS progenitors [15]. As CFU-M progenitors appear in YS before the onset of definitive hematopoiesis in E10.5 AGM, we used timed fate-mapping approaches at E8.5 and E9.5 to study their embryonic origins. Female *Cx3cr1*$^{CreER\text{-}YFP}$ mice, which express Cre recombinase under control of the *Cx3cr1* promoter upon exposure to TAM, were crossed to male *Rosa*^{tdTom} mice [15]. Pregnant dams were administered TAM at E8.5 or E9.5 to induce irreversible expression of the tdTom reporter in CX_3CR1^+ cells and their progeny. Whereas previous studies have focused on the macrophage [11, 15] or endothelial fate [28, 29] of YS progenitors, we tracked both lineages in aorta together with CFU-M progenitors. After E8.5 induction, adult aorta contained $tdTom^+$ cells that included all three populations, with macrophages being most prevalent, followed by progenitors (**Supplemental Figure S6A, B**). For E9.5 induction, we first confirmed that there was negligible labeling of cells in BM at 12 w, the main site of definitive hematopoiesis postnatally (**Figure 3A**). Whereas CFU-M from E15.5 liver and adult BM were exclusively $tdTom^-$, $tdTom^+$ CFU-M were produced by E15.5 AGM cells and 12 w aortic cells, indicating their origins from an E9.5 CX_3CR1^+ source

(**Figure 3B**). In keeping with this, we identified tdTom$^+$ progenitors, as well as tdTom$^+$ macrophages and endothelial cells in both E15.5 AGM and 12 w aorta, although tdTom$^+$ progenitors were less frequent postnatally (**Figure 3C, D**). After normalizing tdTom labeling to results for brain microglia, E9.5 CX$_3$CR1$^+$ cells accounted for the source of ~43% of progenitors, ~32% of macrophages and ~16% of endothelial cells in 12 w aorta, while making negligible contribution to monocytes in blood or aorta (**Figure 3E, F**). Immunofluorescent confocal microscopy also confirmed the presence of intimal and adventitial tdTom$^+$CDH5$^+$ endothelial cells, and adventitial tdTom$^+$CD68$^+$ macrophages and tdTom$^+$c-Kit$^+$ progenitors in aortas of E9.5 TAM-induced adult *Cx3cr1*$^{\text{CreER-YFP}}$ x *Rosa*^{tdTom} mice (**Figure 3G**).

Complementary fate-mapping was performed by giving TAM to *Csf1r*$^{\text{Mer-iCre-Mer}}$ x *Rosa*$^{\text{mT/mG}}$ mice at E8.5 to induce GFP expression in YS CSF1R$^+$ cells, including EMPs and their progeny [14]. Approximately 30% of CFU-M from 12 w aorta were GFP$^+$, compared to <2% from donor-matched BM (**Supplemental Figure S6C**). Using flow cytometry, we identified GFP$^+$ progenitors, macrophages and endothelial cells in adult aorta (**Supplemental Figure S6D**). After normalizing to labeling of microglia, ~44% of progenitors, ~26% of macrophages and ~12% of endothelial cells in adult aorta were from an E8.5 CSF1R$^+$ source, consistent with YS EMP origins (**Supplemental Figure S6E, F**). Immunolabeling and confocal microscopy also demonstrated GFP$^+$ cells in ascending and descending aorta, comprising intimal and adventitial CD31$^+$ endothelium and adventitial c-Kit$^+$ progenitors and CD68$^+$ macrophages (**Supplemental Figure S6G, H**).

We next used FACS to isolate embryonically derived tdTom$^+$ or GFP$^+$ progenitors, macrophages and endothelial cells from aortas of E9.5 TAM-induced 12 w *Cx3cr1*$^{\text{CreER-YFP}}$ x *Rosa*^{tdTom} mice or E8.5 TAM-induced 12 w *Csf1r*^{MerCreMer} x *Rosa*$^{\text{mT/mG}}$ mice, respectively

(**Supplemental Figure S7A, B**). Wright-Giemsa staining showed that progenitors had rounded morphology with smooth surface membrane and lacked the protrusions and intracellular vacuolations of macrophages (**Supplemental Figure S7C**). Although they had similarly sized nuclei as macrophages, progenitors had less cytoplasm and a higher nuclear:cell area ratio (**Supplemental Figure S7C**). CFU-M were only produced by progenitors and not macrophages or endothelial cells after culture in methylcellulose (**Supplemental Figure S7D**). These data collectively indicate that aortic CFU-M progenitors originate from an early embryonic $CSF1R^+$ and CX_3CR1^+ source.

CFU-M progenitors have endothelial and macrophage differentiation potential

We next studied the differentiation capacity of aortic progenitors to determine whether they can contribute to the postnatal renewal of embryonically derived macrophages and endothelium. Progenitors, macrophages and endothelial cells were FACS-isolated from freshly digested 12 w C57BL/6J aortas and cultured in Matrigel™ with endothelial growth medium. Whereas primary aortic macrophages displayed no cord forming activity, endothelial cells produced branching cord structures by day 7 (**Supplemental Figure S8A**), with flow cytometry verifying their content to be $CD45^-CDH5^+$ endothelial cells (**Supplemental Figure S8B**). Meanwhile, donor-matched aortic progenitors formed clusters by day 3, which sprouted and gave rise to complex cord networks by day 7, showing different morphology but similar overall cord length to those formed by primary endothelial cells (**Supplemental Figure S8A**). Flow cytometry analysis of these networks showed that progenitors had produced a mixture of new $CD45^+CD11b^+F4/80^+$ macrophages and $CD45^-CDH5^+$ endothelial cells, with some remaining progenitors (**Supplemental Figure S8C**).

This assay was then repeated using progenitors isolated from adult aortic CFU-M. Culture-

derived progenitors produced similar cord networks as freshly sorted progenitors (**Supplemental Figure S8D**). In most donor mouse replicates, these contained a mixture of newly formed endothelial cells and macrophages as determined by flow cytometry (**Supplemental Figure S8E, F**). In addition to losing surface expression of CD45 and gaining CDH5, the endothelial progeny of progenitors also acquired TIE2 (~80%) and VEGFR2 (~40%) expression (**Supplemental Table S1**). Meanwhile, the macrophages produced were mostly CX_3CR1^+ and $CD206^+$ (~75%), with ~45% expressing LYVE-1 and only ~5% MHCII or CCR2 (**Supplemental Table S1**). We also labeled cytospin preparations of these cord networks with antibodies against EMCN and CD68 for confocal microscopy. This verified that progenitors had produced both $EMCN^+$ endothelial cells and $CD68^+$ macrophages, further supporting their bipotency (**Supplemental Figure S8G**).

The bipotent capacity of aortic CFU-M progenitors was then studied at the clonal and single-cell levels. First, we harvested and disaggregated individual CFU-M and replated their cellular content in separate wells in Matrigel™ for 7 d. Progenitors from single CFU-M formed sprouting networks, which contained both macrophages and endothelial cells (**Figure 4A**), demonstrating that bipotency was contained at the clonal level. We then performed single-cell differentiation experiments. CFU-M were grown from adult UBI-GFP (GFP^+) and C57BL/6J (GFP^-) aortas, individually isolated and disaggregated into single-cell suspensions. We seeded a single GFP^+ progenitor with pooled GFP^- progenitors in the same well and co-cultured in Matrigel™ for 7 d. Fluorescence microscopy showed formation of multicellular GFP^+ sprouts from single-cell origins in multiple replicate experiments (**Figure 4B**). Cytospin preparations of each well were labeled for GFP, EMCN and CD68. Five of eleven wells contained both GFP^+EMCN^+ endothelial cells and GFP^+CD68^+ macrophages (**Figure 4B** and **Supplemental Figure S9A, B**), while three had only GFP^+EMCN^+ cells and another three

only GFP$^+$CD68$^+$ cells. Thus, aortic CFU-M progenitors can differentiate into both endothelial and macrophage lineages at the single-cell level.

Macrophage and endothelial transformation of progenitors was also supported by new capacity of these progeny to take up oxidized and acetylated low-density lipoprotein (LDL) cholesterol, respectively, which was not a property of progenitors themselves (**Figure 4C**, **D**). As was the case for 2° renewal, the cord-forming capacity of CFU-M progenitors was highest from E9.5 YS and P1 aortas and lower from 12 w and 52 w aortas (**Figure 4E**).

We next examined whether aortic CFU-M progenitors mediate adventitial neovascularization, as occurs during *vasa vasorum* expansion. Angiogenic sprouting assays were performed with rings from ascending thoracic aorta of E9.5 TAM-induced adult *Cx3cr1*$^{\text{CreER-YFP}}$ x *Rosa*^{tdTom} mice. These produced embryonically derived tdTom$^+$ sprouts (**Supplemental Figure S10A, B**), with a higher proportional content of tdTom$^+$ cells compared to whole aorta, as measured by flow cytometry (**Supplemental Figure S10C**). tdTom$^+$ sprouts contained endothelial cells, progenitors and macrophages in decreasing order of abundance (**Supplemental Figure S10D**). We then used aortic rings from adult C57BL/6J mice, from which adventitia had been removed to eliminate sprouting (**Figure 4F**). Seeding them with aortic CFU-M progenitors from adult UBI-GFP mice rescued adventitial angiogenesis with formation of GFP$^+$ sprouts, that contained an abundance of endothelial cells, with a small percentage of macrophages that were predominantly LYVE-1$^+$MHCII$^-$ (**Figure 4G, H** and **Supplemental Table S1**). Together, these data show that embryonically derived progenitors participate in adventitial neovascularization.

To study the fate and vasculogenic capacity of CFU-M progenitors *in vivo*, we performed

adoptive cell transfer experiments. Surgery was performed on 12 w C57BL/6J mice to induce hindlimb ischemia, before injecting the quadriceps and gastrocnemius with CFU-M-derived progenitors from adult aorta or E9.5 YS from UBI-GFP mice (~$1.5x10^4$ cells) or cell-free Matrigel™ (**Figure 5A**). Laser Doppler imaging showed that aortic progenitors improved perfusion recovery over 14 d compared to control (**Figure 5B**), accompanied by increased capillary and arteriolar density in injected muscle (**Supplemental Figure S10E**). At day 14, GFP^+ cells were detected in recipient muscle but not peripheral blood, with flow cytometry revealing that donor progenitors had produced new endothelial cells and macrophages (**Figure 5C, D**). ~80% of the endothelial cells produced by progenitors *in vivo* were $VEGFR2^+$, while most macrophages were again $CX_3CR1^+LYVE\text{-}1^+MHCII^-$, consistent with the characteristic surface marker profile described for embryonically derived tissue-resident macrophages [14, 15] (**Supplemental Table S1**). Confocal microscopy of immunolabeled sections also identified host-perfused, GFP^+ endothelial-lined neovessels, with adjacent clusters of GFP^+CD68^+ macrophages (**Figure 5E**). Similar results for perfusion recovery and endothelial and macrophage fate were obtained after injection of YS progenitors (**Supplemental Figure S10F-H**).

Collectively, the above results identify aortic CFU-M progenitors as vasculogenic EndoMac progenitors. We next examined their renewal capacity and the durability of their progeny *in vivo*. Progenitors from adult UBI-GFP aortas were transplanted into ischemic C57BL/6J hindlimbs as above. 14 d later, we digested the recipient quadriceps and gastrocnemius into single-cell suspensions that were plated in methylcellulose for another 14 d. These generated GFP^+ CFU-M in methylcellulose, from which GFP^+ progenitors were again isolated and used in 2° hindlimb transfer studies (**Figure 5F**). After another 14 d, engrafted GFP^+ cells had again transformed into endothelial cells or macrophages, with a small percentage of residual

progenitors (**Figure 5G**). Similar results were obtained in 1° transfer studies that were followed for eight weeks instead of two (**Figure 5H, I**). These results show that EndoMac progenitors from adult aorta produce durable endothelial and macrophage progeny *in vivo*. Although they do renew, their capacity to do so is finite meaning that their own numbers diminish over time.

EndoMac progenitors exhibit a myelopoietic and vasculogenic transcriptional profile

To examine the cellular composition of progenitors contained within adult aortic CFU-M, we performed scRNA-seq of culture-derived progenitors pooled from two 12 w C57BL/6J mice. After quality control and filtering, transcriptional profiles of 7,966 cells were analyzed and expression of a total of ~26,000 genes was detected (**Supplemental Table S2**). Cluster analysis revealed that CFU-M progenitors were composed of nine clusters of cells, including six closely related clusters (progenitors 1-6), two highly proliferative clusters marked by *Mki67* expression (Prolif progenitors 1 and 2), and a small distinct cluster (progenitors 7) (**Figure 6A-D** and **Supplemental Table S3**). Consistent with the immunophenotype of aortic CFU-M progenitors, all clusters expressed *Ptprc* (CD45), *Kit*, *Ly6a* (Sca-1) and *Pecam1* (CD31), with almost no expression of mature endothelial (*Cdh5*, *Kdr*/Vegfr2, *Tek*/Tie2) or macrophage (*Itgam*/Cd11b, *Adgre1*/F4/80, *Fcgr1*/Cd64, *Lyve1*) genes (**Figure 6E,F**). Near absence of *Flt3* expression reiterated that these cells originate independently of BM hematopoiesis (**Figure 6G**), while expression of *T* (Brachyury) in most cells indicated their origin from embryonic mesenchyme **(Figure 6H**). In keeping with our earlier results, the progenitors did not express pluripotency genes (*Nanog*, *Sox2*, *Pou5f1/Oct4*), although all the clusters expressed the stem cell self-renewal gene *Klf2*, six of the clusters also expressed low levels of *Myc* and in addition, the smallest cluster (progenitors 7) expressed *Klf4* (**Supplemental Figure S11A**). Genes and transcription factors that mark YS EMPs were

expressed in the majority of cells (*Cd93*, *Gata1*, *Gata2*) or at least in some cells in all clusters (*Csf1r*, *Bpnt1*, *Id1*), consistent with their embryonic YS origin (**Figure 6I** and **Supplemental Figure S11B**) [41]. At the same time, all clusters displayed variable levels of expression of *Cx3cr1*, *Zeb2*, *Maf*, *Mrc1* and *Tnfrsf1b* genes, which are upregulated in YS-derived pre-macrophages [41] (**Figure 6I** and **Supplemental Figure S11C**). Additionally, albeit at varying frequencies, all clusters expressed many of the genes involved in myelopoiesis (*Spi1*, *Cd34*, *Myb*, *Mafb*, *Cebpb*, *Nr4a1*) [42-46] and vasculogenesis or angiogenesis (*Gsn*, *S110a6*, *Dcn*, *Runx1*, *Vegfa*, *Flt1*, *Angpt1*, *Epor*) [47-49], while cluster 7 was notable for expressing higher levels of *Flt1*, *Il33*, *Pdgfra*, *Postn*, *Cd248* and *Sox9*, which are upregulated in endothelial progenitor cells [49-51] (**Figure 6I** and **Supplemental Figure 11D,E**). This, in line with our *in vitro* and *in vivo* findings, suggests that CFU-M progenitors are transcriptionally primed for differentiation into myelopoietic and vasculogenic lineages.

Trajectory analysis using Monocle3 revealed a progressive relationship between clusters of cells in pseudotime starting from cluster 1 and ending in proliferative clusters, indicating that they represent different cell states (**Supplemental Figure S11F**). Pathway analysis of gene expression signatures of cellular clusters (**Supplemental Table S4)** showed an overlap of overrepresented pathways among clusters, also suggesting a continuum of cell states (**Supplemental Figure S11G** and **Supplemental Tables S5-13**). Transcription factor binding site analysis of gene expression signatures revealed significant overrepresentation of binding sites for transcription factors involved in the regulation of cell cycle (members of E2F and DP families and Rb), embryonic development (Foxd3 and Sox10), cell fate determination (Sox10), genes in response to injury and inflammation (Nrf2), heart development (Zfp161) and circulatory system development (Hes1), in the differentially expressed genes in one or more clusters (**Supplemental Table S14**). This is consistent with the tissue source,

developmental origin, and properties of these progenitors.

Together, these data demonstrate that aortic CFU-M progenitors are a relatively homogeneous population containing highly proliferative, as well as less proliferative, cells with potency for both macrophage and endothelial lineages and some degree of heterogeneity that is likely attributable to asynchronous cell states.

Regulatory effects of Angiotensin II on aortic EndoMac progenitors

The renin-angiotensin system, and specifically AngII, play key regulatory roles in myelopoiesis [52] and vascular inflammation [53]. When pluripotent stem cells undergo hemato-endothelial differentiation *in vitro*, they transition through bipotent hemangioblasts that form colonies and express ACE (CD143) and the receptors for AngII, AGTR1 and AGTR2 [31]. We found that ACE was expressed on EndoMac progenitors from adult aortic CFU-M *in vitro*, adult aorta *in vivo* and E9.5 YS CFU-M (**Figure 7A-C**). Aortic progenitors also expressed AGTR2 at the cell surface (**Figure 7A**) and at mRNA level (**Figure 7D**), with much lower expression of AGTR1. AngII induced concentration-dependent increases in 1° CFU-M yield from 12 w C57BL/6J aortas (**Figure 7E**). Furthermore, when incubated with 100 nM AngII, aortic CFU-M could be renewed in bulk culture for four passages in much larger numbers compared to control (**Figure 7F**). Conversely, treatment with inhibitors of ACE (enalapril), AGTR1 (losartan) and AGTR2 (PD123,319) showed that inhibition of AGTR1 and AGTR2 reduced 1° CFU-M yield (**Figure 7G**).

Given that AngII rapidly stimulates the accumulation of macrophages in aortic adventitia [54], we next studied how it affects the ability of aortic progenitors to produce macrophages *in vivo*. We made use of the peritoneal cavity as a niche for macrophage expansion by injecting

10^4 progenitors from 12 w UBI-GFP aortas into the peritoneum of C57BL/6J mice, and followed this with daily *i.p.* injections of AngII, M-CSF or PBS (**Figure 7H**). Flow cytometry was used to check the purity of undifferentiated progenitors before injection (**Figure 7I**) and their *de novo* differentiation into CD11b$^+$F4/80$^+$ macrophages on retrieval from the peritoneal cavity 72 h later (**Figure 7J**). AngII promoted expansion of progenitor-derived macrophages by 14.5-fold and 3.4-fold compared to PBS and M-CSF, respectively (**Figure 7J, K**).

In keeping with these different effects of AngII on EndoMac progenitors, qRT-PCR also showed that it upregulated mRNA levels of genes involved in cell division (*Ccna1*, *Ccnb1*, *Ccnd2*), self-renewal (*Myc*, *Nanog*, *Klf4*) [45, 55], myelopoiesis (*Klf4*, *Irf8*) [56], M2-like macrophage polarization (*Arg1*) and endothelial specification and angiogenesis (*Cdh5*, *Cd248*) (**Figure 7L-P**).

EndoMac progenitors expand early in response to AngII-induced aortic inflammation

AngII-induced vascular inflammation is characterized by expansion of adventitial macrophages [54], adventitial fibrosis [57] and in some mouse strains, development of aortic aneurysms [58]. A recent study reported that after 10 d of exposure to AngII, adventitial macrophages expanded due to both recruitment of BM-derived cells and local proliferation of embryonically derived macrophages [36]. As AngII stimulated a marked increase in progenitor-derived macrophages within 72 h in our peritoneal transfer assay, we focused on its early effects on aortic progenitors and macrophages after systemic infusion by osmotic pump. In *Flt3*^{Cre} x *Rosa*$^{mT/mG}$ mice, 48 h of AngII infusion caused a significant 5.8-fold increase in Flt3-Cre$^-$ macrophages compared to PBS control (**Figure 8A, B**), with more Flt3-Cre$^+$ and Flt3-Cre$^-$ macrophages in S-phase of cell cycle (both 2.9-fold vs PBS) (**Figure 8C**). As a potential contributor to the expansion of non-BM derived macrophages, AngII also induced expansion

and proliferation of Flt3-Cre^{-} progenitors, with fold comparisons compared to PBS: 3.0x for aortic CFU-M yield (**Figure 8D**); 8.5x for progenitor number assessed by flow cytometry (**Figure 8E**); and 10.5x for progenitors in S-phase (**Figure 8F**).

We next used adult *Cx3cr1*$^{\text{CreER-YFP}}$ x *Rosa*^{tdTom} mice that had been administered TAM at E9.5, for AngII or PBS infusion by osmotic pump for 12 h, 48 h or 168 h (**Figure 8G**). AngII increased the numbers of tdTom^{+} cells in aorta at 12 h and 48 h compared to PBS (fold difference by flow cytometry: 4.4x at 12 h, 2.6x at 48 h, 1.3x at 168 h) (**Figure 8H**). Confocal microscopy of immunolabeled aortic sections showed a similar expansion of tdTom^{+} cells in the adventitia of descending aorta at 48 h (**Figure 8I**). As measured by aortic CFU-M yield, the AngII-induced expansion of embryonically derived EndoMac progenitors was highest at 12 h (6.1-fold vs PBS), still evident at 48 h (3.3-fold) but no longer at 168 h (1.3-fold) (**Figure 8J**). This was corroborated by flow cytometry, showing that EndoMac progenitors undergo very early expansion in response to AngII (**Figure 8K**).

DISCUSSION

The intimate association between the hematopoietic and endothelial lineages begins early in development. Converging evidence indicates that YS EMPs give rise to both macrophages and endothelial cells in adult mouse tissues [16, 28]. In this study we identify undifferentiated EndoMac progenitors in murine aorta that also originate embryonically. These progenitors are more abundant at birth, at which time they have enhanced clonal capacity and are maintained independently of Flt3^{+} hematopoiesis. As supported by *in vitro* and *in vivo* differentiation studies, they are bipotent for macrophage and endothelial lineages and possess vasculogenic capacity. We also demonstrate a regulatory role for AngII, which stimulates their clonogenic, proliferative and differentiation properties.

Most mature cell types rely on the self-renewal of stem cells and proliferation and differentiation of transient amplifying progenitors for their homeostatic turnover and recovery after tissue insult. Although there has been conjecture about how embryonically derived macrophages are maintained after birth, prevailing opinion favors their ability to self-renew without losing functional or differentiated status [27]. This was initially based on experiments showing self-renewal of macrophages in which MafB and c-Maf were genetically knocked out [44]. Subsequent studies have provided contrasting data either supporting the long-lived nature of tissue-resident macrophages, especially microglia [59], their stochastic turnover [13, 60], repopulation by clonal expansion [61, 62] or differentiation from local progenitors [63]. The mechanistic basis for macrophage self-renewal has been linked to downregulation of MafB/cMaf, which occurs constitutively in some macrophage populations (e.g. alveolar macrophages) or can be induced (e.g. by M-CSF). This in turn activates a self-renewal gene network, centered around *Myc*, *Klf2* and *Klf4* [45].

As shown here, the *in vitro* growth of CFU-M from adult aorta is not due to monocytes or macrophages, but rather embryonically derived progenitors. The finding that CFU-M undergo 2° renewal from single-cell origins paved the way for us to study their composition and identify a $Lin^{-}CD45^{+/Lo}CD11b^{-}F4/80^{-}Sca\text{-}1^{+}c\text{-}Kit^{+}$ fingerprint for progenitors both in culture-derived CFU-M and aorta *in vivo*. This surface phenotype distinguishes EndoMac progenitors from myeloid-committed progenitors in BM, such as macrophage/dendritic cell progenitors and common monocyte progenitors, which lack Sca-1 but express Flt3/CD135 and Ly6C, respectively [64, 65]. As a high percentage of progenitors are actively dividing even in steady state, it is not surprising that their ability to renew is finite and diminishes with aging, along with their clonogenic and angiogenic capacity. Combined with a lack of circulatory renewal from $Flt3^{+}$ BM hematopoiesis, this helps explain why aortic progenitor numbers decrease

postnatally. However, we also demonstrate that their proliferation and renewal can be amplified by stimulatory cues, such as elicited by AngII.

As in previous studies [66], we found negligible contribution from YS EMPs to adult BM hematopoietic cells. As revealed by embryonic profiling across different gestational ages and timed induction of fate-mapping, EndoMac progenitors are present in YS by E8.5 and migrate intra-embryonically to AGM by E10.5. This aligns with prior findings for EMPs and CX_3CR1^+ pre-macrophages [24]. Throughout our differentiation assays, EndoMac progenitors produced macrophages without evidence of passing through a monocyte intermediate stage. This separates them from the EMPs that colonize fetal liver where they produce monocytes and other lineage-committed progenitors [25]. This was reflected here by mixed growth of different CFU types from E12.5-15.5 liver, as distinct from selective CFU-M growth from AGM at the same ages. By scRNA-seq we found that culture-derived progenitors expressed genes transcribed in YS EMPs and pre-macrophages, which places them in an intermediate stage and may explain their ability to directly produce macrophages.

The classical origin of embryonic vascular endothelial cells is the differentiation of mesoderm-derived angioblasts around E7.0 YS in mice [67]. Subsequently, endothelial cells undergo local proliferation during tissue angiogenesis, with evidence for clonal expansion in adult tissues under ischemic insult [68]. Other identified sources of postnatal endothelial renewal include circulating endothelial progenitor cells [69] and tissue-resident endovascular progenitors [51]. Plein *et al*. recently reported that endothelial cells in YS and some embryonic and adult tissues also derive from YS EMPs [28], although this was not reproduced by another study [29]. In tracking the fate of E8.5 and 9.5 CX_3CR1^+ and E8.5 $CSF1R^+$ progenitors, we examined both their macrophage and endothelial progeny. In support of Plein's study, we

identified embryonically derived endothelial cells in postnatal aorta. Although it has been widely accepted that embryonically derived macrophages and endothelium are maintained after birth by proliferative self-renewal, another explanation could be the postnatal transformation of EndoMac progenitors into these two distinct lineages. We observed this to occur across different *in vitro* and *in vivo* experiments with overrepresentation of implicated signaling pathways and expression of myelopoietic and vasculogenic genes *in vitro*. Although our results suggest that these progenitors have a differentiation bias toward the endothelial lineage in the settings of adventitial vasculogenesis and post-ischemia repair, they can also rapidly generate macrophages, as seen here after peritoneal injection. Importantly, they appear predisposed to forming macrophages that are LYVE-1^{+}MHCII$^{-/Lo}$CCR2^{-}, in keeping with the identity of embryonically derived macrophages that reside in the aortic adventitia and other tissues [15, 36, 39].

The century-old notion of the hemangioblast, a bipotent progenitor for endothelial and hematopoietic cells in development [30], has been supported by *in vitro* evidence of a common pathway for hemato-endothelial differentiation from pluripotent stem cells [31, 32, 70]. Here, we observed by scRNA-seq that EndoMac progenitors express the canonical hemangioblast gene, *T* (Brachyury), while they also exhibited surface expression of ACE and AGTR2, which too are linked to hemato-endothelial bipotency [31]. Focusing our attention on AngII as a regulator of their properties, we found that AngII stimulated the proliferative, clonogenic and macrophage-forming capacity of aortic EndoMac progenitors, and upregulated various genes, such as *Nanog*, *Myc*, *Irf8* and *Arg1*. Together with our results from short-term AngII infusion in *Flt3*^{Cre} and *Cx3cr1*^{CreER} mice, this indicates that these progenitors are primed to provide an immediate proliferative response to AngII. This may help feed the local expansion of adventitial macrophages and endothelial cells, which is complemented by recruitment and

proliferation of BM-derived macrophages, which also contribute to AngII-induced adventitial inflammation [36].

In conclusion, our discovery of aortic EndoMac progenitors adds to the recognized fate of early embryonic progenitors in postnatal tissues. These bipotent progenitors can rapidly proliferate and differentiate to drive adventitial neovascularization. Their existence also provides a new model to help explain the local maintenance and expansion of embryonically derived tissue-resident macrophages and endothelial cells after birth.

METHODS

Resource availability

Details of general reagents are provided in **Supplemental Table S15**. Further information and requests for resources and reagents should be directed to and will be fulfilled by the lead contact, Peter Psaltis (peter.psaltis@sahmri.com).

Data and code availability

The single-cell RNA-seq (scRNA-seq) data has been deposited in the National Centre for Biotechnology Information Gene Expression Omnibus [71] and is accessible through GEO Series accession number GSE232625 (https://www.ncbi.nlm.nih.gov/geo/query/acc.cgi?&acc=GSE232625).

All other data will be made available upon request.

Experimental details

Mouse models

x3cr1$^{GFP/+}$ (B6.129P-Cx3cr1^{tm1Litt}/J), *Ccr2*$^{-/-}$ (B6.129S4-Ccr2^{tm1Ifc}/J), *Rosa*^{mTmG}

(Gt(ROSA)26Sor$^{tm4(ACTB-tdTomato,-EGFP)Luo}$/J), *Csf1r*$^{Mer-iCre-Mer}$ (FVB-Tg(Csf1r-cre/Esr1*)1Jwp/J), *Cx3cr1*$^{YFP-creER}$ (B6.129P2(Cg)-Cx3cr1$^{tm2.1(cre/ERT2)Litt}$/WganJ) and ubiquitous GFP (UBI-GFP) (C57BL/6-Tg(UBC-GFP)30Scha/J) mice were purchased from The Jackson Laboratory. C57BL/6J mice were from the South Australian Health and Medical Research Institute (SAHMRI). Male *Flt3*^{Cre} breeding mice were initially provided by Professors Thomas Boehm (Max-Plack-Institute of Immunobiology and Epigenetics, Freiburg, Germany) and Toshiaki Ohteki (Tokyo Medical and Dental University, Tokyo, Japan). A breeding colony of *Rosa*^{tdTom} (B6.Cg-*Gt(ROSA)26Sor*$^{tm14(CAG-tdTomato)Hze}$/J) mice was provided by Dr Daniel Worthley (Precision Medicine Theme, SAHMRI). *Cx3cr1*$^{GFP/+}$ mice were inter-crossed to obtain *Cx3cr1*$^{GFP/GFP}$ mice. *Flt3*^{Cre} and *Csf1r*$^{Mer-iCre-Mer}$ mice were crossed with *Rosa*^{mTmG} mice to obtain *Flt3*^{Cre} x *Rosa*^{mTmG} and *Csf1r*$^{Mer-iCre-Mer}$ x *Rosa*^{mTmG} mice, respectively. *Cx3cr1*$^{YFP-creER}$ mice were crossed with *Rosa*^{tdTom} mice to obtain *Cx3cr1*$^{CreER-YFP}$ x *Rosa*^{tdTom} mice. *Csf1r*$^{Mer-iCre-Mer}$ mice were maintained on FVB and C57BL/6J mixed background. All mice were housed in a temperature and humidity-controlled environment under a 12-hour light/dark cycle with *ad libitum* access to water and standard chow diet. Male and female mice were used in all experiments and experimental arms were gender- and age-matched, except for *Flt3*^{Cre} x *Rosa*^{mTmG} fate-mapping studies where only males were used as the Flt3-cre modification is located on the Y chromosome. All animals were treated in accordance with the Australian Code of Practice for the Care and Use of Animals for Scientific Purposes and were approved by the SAHMRI Animal Ethics Committee (ID SAM117, SAM155, SAM308 and SAM432.19).

To achieve Cre-Lox recombination in *Cx3cr1*$^{CreER-YFP}$ x *Rosa*^{tdTom} and *Csf1r*$^{Mer-iCre-Mer}$ x *Rosa*^{mTmG} mice, 75 µg/g of 4-hydroxytamoxifen (TAM, Sigma-Aldrich) was intraperitoneally (*i.p.*) injected into pregnant dams at either E8.5 or E9.5, as specified. To analyze the cell cycle

state of progenitors in aorta, 1 mg of bromodeoxyuridine (BrdU) was injected *i.p.* before euthanasia and tissues harvested at specified times.

Preparation of single-cell suspensions

Experiments were performed with freshly isolated, single cell disaggregates from tissues, as specified. Aortas were dissected out intact, along the entire length from aortic valve to iliac bifurcation and flushed extensively with PBS, before microscopic dissection of surrounding perivascular fat and, where indicated, careful separation of the adventitia. The aorta was digested with Liberase™ (50 µg/mL) (Roche Applied Science) for 1.5 h at 37°C. Tissue digests were then passed through a 40-µm nylon mesh (Greiner Bio-One) and neutralized with Iscove's Modified Dulbecco's Medium (IMDM, Sigma-Aldrich) supplemented with 10% fetal bovine serum (FBS, Cell Sera).

Where applicable, single cell disaggregates were also prepared from the liver, quadriceps and gastrocnemius muscle, brain, blood, BM and spleen. Liver and muscle tissues were digested with Liberase as per the aortas to give single-cell suspensions. The brain was carefully removed from cephalic mesenchyme and meninges, dissected out, minced, and incubated in Liberase™ (50 µg/mL) for 2 h and passed through a 40-µm nylon mesh [72]. Digests of brain were resuspended in 37% isotonic Percoll, underlaid with 70% isotonic Percoll (GE Healthcare), centrifuged (600 *g*, 25 min) and cells in the interface were collected. Blood was collected by cardiac puncture in EDTA coated blood collection tubes. Erythrocytes were lyzed by mixing with ammonium chloride (1:10 v/v; StemCell Technologies) at 4°C for 10 min, then non-erythroid blood cells were washed and centrifuged (300 *g*, 5 min). BM cell suspensions were prepared by flushing femurs and tibias with PBS. Spleens were homogenized through a 40-µm cell strainer. BM and spleen cell suspensions were incubated

in ammonium chloride at 4°C for 8 min, following which cells were washed and centrifuged (400 *g*, 5 min).

Gestational embryonic age was defined based of the date of vaginal plug formation, which was set at E0.5. To obtain single cell disaggregates from embryos, pregnant females were euthanized by CO_2 exposure. Each embryo was carefully dissected from the uterus under a dissection light microscope (Carl Zeiss); tissues harvested were YS (E7.5-E15.5), whole embryo (E7.5-E9.5), AGM (E10.5-E15.5) and liver (E11.5-E15.5) [73]. Tissues were washed with PBS and placed in Hanks balanced-salt solution (HBSS, Sigma) supplemented with 2% FBS and digested with 1 mg/mL of collagenase II for 15 min at 37°C. Tissue suspensions were filtered using Polystyrene Round-Bottom Tubes with Cell-strainer cap strainers (In Vitro Technologies) and centrifuged (400 *g*, 5 min).

All single-cell suspensions were resuspended in IMDM supplemented with 10% FBS and 1% antimycotic/antibiotic solution, before performing total cell counts for colony-forming unit (CFU) assays or flow cytometric characterization.

Clodronate monocyte depletion

To deplete circulating monocytes, clodronate (clodronateliposomes.org, Vrije Universiteit, Netherlands) was injected *i.p.* into 12 w C57BL/6J mice daily for two days, while vehicle (PBS) control liposomes were used as control.

Hematopoietic colony-forming unit (CFU) assays

Clonogenicity was assessed by performing CFU cultures. Briefly, $2x10^5$ freshly isolated cells from digests of aorta or specified tissue were plated in methylcellulose (MethoCult GF

M3434, StemCell Technologies), in duplicate. Where specified, cultures were performed in the presence or absence of Fractalkine (CX_3CL1) (100 nM; Sigma-Aldrich), M-CSF (50 nM; PeproTech), AngII (10 nM, 100 nM, 1000 nM; Sigma-Aldrich), Enalapril (100 nM; Sigma-Aldrich), Losartan (100 nM; Sigma-Aldrich) or PD123,319 (50 nM; Sigma-Aldrich), which were replenished every three days. After 14 d, CFUs (defined as a minimum of 30 cells) were counted under light microscopy and classified by colony subtype (e.g. CFU-M) and size, as described previously [34, 35]. In some experiments, after completion of CFU counts on day 14, colonies were isolated and disaggregated into single-cell suspensions for CFU-M renewal assays, flow cytometric characterization or other experiments as specified.

CFU renewal assays were performed by individually isolating 1° or 2º CFU-M from methylcellulose under light microscopy. Isolated colonies were then disaggregated, and single cells re-plated in methylcellulose in 96-well plates. Wells were imaged daily until day 14 to document and quantify the emergence of new colonies in 2º and 3º cultures from each plated cell.

CFU-M were also passaged in the presence or absence of 100 nM AngII in bulk culture. For this, the methylcellulose from 1° cultures was liquefied and disaggregated to obtain a single-cell suspension, which was then re-cultured in methylcellulose at a density of $2x10^5$ per well of a 24-well plate, for another 14 d before colony counting. Further passages (tertiary, quaternary, quinary) were conducted in the same way.

Flow cytometry and cell sorting

Single-cell suspensions from tissue digests or culture-derived CFU-M were resuspended in aliquots of $\leq 10 \times 10^6$ cells/mL in PBS/5% FBS/0.2% sodium azide. 1 µL of fixable viability

stain 700 (BD Horizon) was added to each sample and incubated for 15 min on ice. After washing, samples were blocked with purified rat anti-mouse CD16/CD32 (BD Pharmingen, San Diego CA, USA) antibody for 5 min on ice. Cells were then incubated for 30 min with 1º antibodies and subsequently with 2º antibodies when required (**Supplemental Table S15**). Samples were then washed and fixed in formalin/PBS for analysis with BD LSRFortessa™ X-20 and BD FACs Diva Software (BD Biosciences) or Cytek® Aurora and SpectroFlo® software (Cytek Biosciences). For cell cycle analysis, BrdU Flow Kit (BD Biosciences) was used as per manufacturer's instructions.

Data files were analysed using FlowJO version X software (Tree Star Inc., Ashland, OR, USA). Gating was performed based on SSC-A vs FSC-A (to exclude cell debris), FSC-H vs FSC-A (for single cells) and the use of Fixable Viability Stain 700 (BD Biosciences). We used FMO controls for each experiment to determine the positive percentage expression of different surface markers. A FACSFusion cell sorter (BD Bioscience) was used for cell sorting.

Matrigel™ cord-forming assay

FACS-sorted progenitors, macrophages and endothelial cells from 12 w C57BL/6J aortas, and progenitors isolated from day 14 medium-sized CFU-M were suspended in Endothelial Cell Growth Medium (Lonza, Cat# CC-4542) and plated on growth factor-reduced Matrigel™ (BD Biosciences) at $2x10^4$ cells per well of a 96-well plate, to study their intrinsic capacity to form vascular-like cords. Cultures were photographed under a light microscope daily until day 7 to detect the presence of cords, identified as cellular extensions linking cell masses or branch points. Images were captured at 10x magnification in five different regions spanning the entire well. Total cord length and number of branching points were quantified using

Image J software (NIH). Single-cell suspensions were retrieved from the Matrigel™ following digestion with type IV collagenase (Sigma-Aldrich) for 45 min, neutralized with IMDM supplemented with 10% FBS, and immunostained for flow cytometry, as published [50].

For the single-cell differentiation assay, progenitors isolated from day 14 aortic CFU-M from UBI-GFP mice were disaggregated and serially diluted in Endothelial Cell Growth Medium to obtain a single GFP^+ cell. A single GFP^+ cell was plated on 15 µL of Matrigel™ with $2x10^4$ GFP^- CFU-M-derived progenitors from C57BL/6J aortas per well in a µ-slide angiogenesis (ibidi®, cells in focus) and cultured for 7 d. Cultures were imaged on a Leica TCS SP8X/MP laser scanning confocal microscope (Leica Microsystems) on day 0 to demonstrate the presence of a single GFP^+ cell in each well, and then on day 7 to determine its differentiation. Single-cell suspensions were prepared from Matrigel™ cultures as described above. 100 µL of cell suspension from each well was placed in a Shandon single cytofunnel (EPKM5991040, Epredia™) and centrifuged onto coated cytoslides (EPKM5991056, Epredia™) in a Shandon Cytospin®4 Cytocentrifuge (Life Technologies, CA, US) (1000*g*, 5 min) for cytospin preparations for immunolabeling.

Aortic ring outgrowth model

Aortic ring assays were used to study the involvement of aortic EndoMac progenitor cells in adventitial angiogenesis. Aortic explants were carefully flushed to remove blood and dissected free of surrounding adipose. For studies from *Cx$_3$cr1*$^{CreER\text{-}YFP}$ x *Rosa*^{tdTom} mice which required intact adventitia, aortas were used with all three mural layers intact. For studies that required addition of GFP^+ aortic EndoMac progenitors, C57BL/6J aortas were dissected to completely remove the adventitia. Rings of 1 mm thickness were then cut from ascending thoracic aorta, embedded in Matrigel™ and overlaid with Endothelial Cell Growth

Medium. Aortic sprouts were imaged on day 7 for quantification of adventitial sprout length using Image J software. Single-cell suspensions were retrieved from adventitial sprouts in Matrigel™ as described above, and immunostained for flow cytometry.

Wright-Giemsa staining

FACS-sorted progenitors, macrophages and endothelial cells from aortas of E9.5 TAM-induced 12 w *Cx3cr1*$^{\text{CreER-YFP}}$ x *Rosa*^{tdTom} mice or E8.5 TAM-induced 12 w *Csf1r*$^{\text{Mer-iCre-Mer}}$ x *Rosa*^{mTmG} mice were resuspended in 200 µL of IMDM containing 2% FBS. Cells were cytospun (300 *g*, 5 min) onto cytoslides using a cytospin centrifuge (Thermo Fisher) and then stained with Wright-Giemsa reagent (Sigma-Aldrich) followed by imaging on a light microscope (Carl Zeiss, Axio).

Immunofluorescence labeling and confocal microscopy

Intact tissue samples were harvested from mice and placed in 30% sucrose overnight, fixed with 10% formalin for 24 h then embedded in Optimal Cutting Temperature (O.C.T.) compound (Sakura Finetek). Five µm thick frozen sections were cut, fixed and then placed in methanol with 0.3% H_2O_2 before heat-mediated citrate antigen retrieval. Blocking was performed with either 10% normal goat or donkey serum, or 3% normal horse serum. Sections were incubated with 1° antibodies overnight followed by 2° antibodies (**Supplemental Table S15**). Nuclei were counterstained with DAPI. Microscopy was performed with a Leica TCS SP8X/MP laser scanning confocal microscope (Leica Microsystems).

For labeling of cytospun preparations, slides were fixed in 4% paraformaldehyde (PFA) for 10 min. Permeabilization was performed with 0.1% Triton X-100 and blocking with 5% normal

horse serum (NHS) for 30 min each, and then hybridization with 1º antibody overnight at 4ºC followed by 2º antibody for 45 min at 37ºC. All antibodies were diluted in 1% NHS. Nuclei were counterstained with DAPI. Confocal microscopy was performed as above. Images were taken from 20-25 fields of view to image all cells and analyzed using ImageJ software.

Hindlimb ischemia model

For adoptive cell transfer studies, we used male and female 12 w C57BL/6J mice as recipients and UBI-GFP mice as donors. To induce hindlimb ischemia, the proximal portion of the left femoral artery and the distal saphenous artery were both ligated, as well as the popliteal artery and all branches in between, and an arterectomy performed to remove the intermediate segment of vessel. Purity checked EndoMac progenitor cells isolated from medium CFU-M grown from either adult aortic cells or E9.5 YS cells from UBI-GFP donor mice ($7.5x10^3$ in 60 µL Matrigel™) were administered as three intramuscular injections into the quadriceps and gastrocnemius of the ischemic limb. A control group received injections of cell-free Matrigel™.

Hindlimb blood flow reperfusion was determined by laser Doppler perfusion imaging (moorLD12-IR, Moor Instruments) immediately following surgery and then at days 7 and 14 post-ischemic induction. Euthanasia was performed after the final imaging on day 14. Peripheral blood was taken by cardiac puncture, while the quadriceps and gastrocnemius muscle from both hindlimbs was harvested and processed for hematopoietic CFU assays, flow cytometry or immunofluorescence staining, to detect engraftment of donor GFP^+ cells, their fate and vasculogenic capacity.

Single-cell RNA sequencing and data analysis

Single-cell RNA sequencing was performed on viable ($DAPI^+$) aortic CFU-M progenitors grown from two 12 w C57BL/6J male mice. Isolated progenitors were subjected to MULTI-seq labeling as previously described [74]. Briefly, cells were resuspended in 18 µL of 1X PBS, labeled with a unique 2 µM anchor lipid-modified oligonucleotide (LMO)-Barcoded Oligo complex for 5 min on ice. After this incubation, 2 µM co-anchor was added and cells incubated on ice for another 5 min. Labeling was quenched with 1 mL of PBS + 2% BSA and cells from each sample in the run mixed for washing the pool with PBS + 1% BSA (twice); final resuspension was in PBS + 1% BSA. From pooled cells, single cell sequencing libraries were prepared using the Chromium Next GEM single-cell 3' kit (v3.1, 10x Genomics) and Chromium system (10x Genomics) according to manufacturer's specifications, at the South Australian Genomics Centre (SAGC, SAHMRI, Adelaide). Paired-end sequencing was performed first, on an Illumina Nextseq High using v2 chemistry, at the SAGC, and subsequently, to increase read depth, on an Illumina Novaseq 6000 (Illumina, San Diego, USA) using one lane of an S4 flowcell (Illumina), at the Australian Genome Research Facility (AGRF, Melbourne, Australia).

Cell Ranger v7.0.0 (10x Genomics) was used to process raw sequencing data from the two runs before subsequent analyses. This pipeline aligned sequencing reads from FASTQ files to the mm10 transcriptome using the STAR aligner and quantified the expression of genes in each cell. FASTQ files from the two sequencing runs were then combined and cell ranger analysis performed on combined FASTQ files to quantify gene expression and barcode enrichments per cell. The Seurat demultiplexing pipeline [75] was applied to demultiplex cells to their original sample-of-origin. Cells detected with zero barcodes (Negatives) or more than one barcode (Doublets) were discarded in this analysis. From the remaining 16,350 singlets,

cells containing expression values for <200 genes or >9000 genes were filtered out as initial quality control measures. Moreover, cells with more than 20% of mitochondrial genes were filtered out to exclude low-quality and dying cells, which often exhibit extensive mitochondrial contamination. These resulted in 16,088 singlets corresponding to three barcodes, BC1: aortic CFU-M population (7,977 cells), BC2: Study population 2 (4,795 cells), and BC3: Study population 3 (3,316 cells). The data from the latter two populations will be published elsewhere. A further quality control measure of 10% mitochondrial gene cut-off was applied to the aortic CFU-M population. The remaining cells were then used to characterize the cellular heterogeneity of CFU-M progenitors. Processed scRNA-seq data was analysed in R v4.1.3 using the Seurat R package v4.1.1 [75].

Dimensionality reduction was performed using Principal Component Analysis to explore transcriptional heterogeneity and perform clustering of cell types. Twenty principal components (PCs) were selected based on the elbow plot. PC loadings were used as inputs for a graph-based approach to cluster cells by cell type with resolution 0.6, and as inputs for Uniform Manifold Approximation and Projection (UMAP) for visualization purposes. Marker genes for each cluster were identified using "FindAllMarkers" R function. Phylogenetic tree relating the 'average' cell from each CFU-M identity class was constructed using "BuildClusterTree" R function. Ggtree R package [76] was then used for visualization and annotation of the CFU-M cluster tree. Trajectory analysis was performed using Monocle 3 [77-79] as described in http://cole-trapnell-lab.github.io/monocle3/. Monocle 3 R package offers trajectory analysis to model the relationships between groups of cells as a trajectory of gene expression changes. The pseudotime, a measure of progression over trajectory, was calculated with CFU-M trajectory starting from Progenitors 1. The graph test function of Monocle was

utilized to identify genes that vary over the CFU-M trajectory. Figures were primarily generated using Seurat, ggplot2 [80] and ggtree R packages.

Bioinformatic analysis of marker genes for each cluster was performed using Innate DB. To identify pathways and transcription factor binding sites associated with marker genes, pathway, and transcription factor binding site overrepresentation analyses were performed using the hypergeometric algorithm and Benjaminin & Hochberg correction for multiple testing with FDR of 0.05.

Gene expression analysis by RT-PCR

Total RNA was extracted from 12 w C57BL/6J aortic digests or aortic CFU-M progenitors, including after exposure to AngII, using Total RNA kit (Bio-Rad). 200 ng of total RNA was reverse transcribed using iScript cDNA synthesis kit (Bio-Rad). Quantitative real-time PCR was performed using the SsoAdvanced™ Universal SYBR® Green RT-PCR Kit (Bio-Rad) on a CFX96 thermocycler (Bio-Rad). Relative changes in target gene expression were normalized using the $^{\Delta\Delta}$Ct method to the housekeeping gene *Actb* (β-actin) and the experimental control condition. Primer sequences used in this study are listed in **Supplemental Table S16**.

Peritoneal transfer assay

Progenitor cells were isolated from medium CFU-M grown from 12 w UBI-GFP aortas and checked for purity. 1 x 10^4 GFP^+ progenitors were injected into the peritoneal cavity of 12 w C57BL/6J mice, which were then randomised and received daily *i.p.* injections of either PBS, 0.7 mg/kg AngII or 0.05 μg M-CSF. Mice were euthanized after 72 h and cells harvested from the peritoneal cavity by injecting 5 mL of PBS *i.p.*. Following gentle massage of the

peritoneum, the peritoneal fluid was collected and centrifuged (400 *g*, 5 min) to obtain single-cell suspensions for immunostaining and analysis of GFP^+ cells by flow cytometry.

Angiotensin II infusion studies

Osmotic minipumps containing AngII (0.7 mg/kg/d) or equivalent volume of PBS, were implanted subcutaneously between the shoulder blades of E9.5 TAM-induced adult *Cx3cr1*$^{CreER\text{-}YFP}$ x *Rosa*^{tdTom} mice or adult *Flt3*^{Cre} x *Rosa*^{mTmG} mice, randomly selected for treatment. Cohorts of mice were euthanized at specified time-points.

Statistical analysis

Results are reported as per the ARRIVE guidelines [81]. Where relevant, data analysis was performed blinded to study group. Statistical analyses were performed using Prism (GraphPad). Data sets were tested for normality of distribution by Shapiro-Wilk test. The ROUT method was applied to identify and exclude any outliers, with Q set to 1%. Statistical comparisons were performed with parametric or non-parametric unpaired or paired two-sample *t*-tests or ANOVA (with post-test multiple comparisons), as specified. Results are expressed as mean ± standard deviation of multiple experiments. In all cases, statistical significance was established at two-tailed $p < 0.05$. The statistical parameters and the number of mice used per experiment are given in the figure legends.

ACKNOWLEDGEMENTS

The authors thank Adelaide Microscopy at the University of Adelaide and staff of the Bioresources Facility, Flow Cytometry Core Laboratory and South Australian Genomics Centre of the South Australian Health and Medical Research Institute, especially Mr Randall Grose and Mr Mark Van der Hoek.

SOURCES OF FUNDING

This work was supported by the National Health and Medical Research Council of Australia [PG 1086796, IG 2001541, PRF 1111630 to S.J.N., CDF 1161506 to P.J.P.]; the National Heart Foundation of Australia [VG 102981, Lin Huddleston Fellowship to C.A.B., FLF 100412, 102056 and 106656 to P.J.P.]; and the Royal Australasian College of Physicians.

DISCLOSURES

S.J.N. has received research support from AstraZeneca, Amgen, Anthera, Eli Lilly, Esperion, Novartis, Cerenis, The Medicines Company, Resverlogix, InfraReDx, Roche, Sanofi-Regeneron and Liposcience and is a consultant for AstraZeneca, Akcea, Eli Lilly, Anthera, Kowa, Omthera, Merck, Takeda, Resverlogix, Sanofi-Regeneron, CSL Behring, Esperion and Boehringer Ingelheim. P.J.P. has received research support from Abbott Vascular, consulting fees from Amgen, Eli Lilly, Esperion and Novartis, and speaker honoraria from Amgen, AstraZeneca, Bayer, Boehringer Ingelheim, Merck Schering-Plough, Pfizer, Novartis and Sanofi.

REFERENCES

1. Qian BZ and Pollard JW. Macrophage diversity enhances tumor progression and metastasis. *Cell*. 2010;141:39-51.

2. Fantin A, Vieira JM, Gestri G, Denti L, Schwarz Q, Prykhozhij S, Peri F, Wilson SW and Ruhrberg C. Tissue macrophages act as cellular chaperones for vascular anastomosis downstream of VEGF-mediated endothelial tip cell induction. *Blood*. 2010;116:829-40.

3. Gurevich DB, Severn CE, Twomey C, Greenhough A, Cash J, Toye AM, Mellor H and Martin P. Live imaging of wound angiogenesis reveals macrophage orchestrated vessel sprouting and regression. *EMBO J*. 2018;37.

4. Cahill TJ, Sun X, Ravaud C, Villa Del Campo C, Klaourakis K, Lupu IE, Lord AM, Browne C, Jacobsen SEW, Greaves DR, et al. Tissue-resident macrophages regulate lymphatic vessel growth and patterning in the developing heart. *Development*. 2021;148.

5. He H, Xu J, Warren CM, Duan D, Li X, Wu L and Iruela-Arispe ML. Endothelial cells provide an instructive niche for the differentiation and functional polarization of M2-like macrophages. *Blood*. 2012;120:3152-62.

6. van Furth R and Cohn ZA. The origin and kinetics of mononuclear phagocytes. *J Exp Med*. 1968;128:415-35.

7. Taoudi S, Gonneau C, Moore K, Sheridan JM, Blackburn CC, Taylor E and Medvinsky A. Extensive hematopoietic stem cell generation in the AGM region via maturation of VE-cadherin+CD45+ pre-definitive HSCs. *Cell Stem Cell*. 2008;3:99-108.

8. Boisset JC, van Cappellen W, Andrieu-Soler C, Galjart N, Dzierzak E and Robin C. In vivo imaging of haematopoietic cells emerging from the mouse aortic endothelium. *Nature*. 2010;464:116-20.

9. Medvinsky A, Rybtsov S and Taoudi S. Embryonic origin of the adult hematopoietic system: advances and questions. *Development*. 2011;138:1017-31.

10. Ginhoux F, Greter M, Leboeuf M, Nandi S, See P, Gokhan S, Mehler MF, Conway SJ, Ng LG, Stanley ER, et al. Fate mapping analysis reveals that adult microglia derive from primitive macrophages. *Science*. 2010;330:841-5.

11. Schulz C, Gomez Perdiguero E, Chorro L, Szabo-Rogers H, Cagnard N, Kierdorf K, Prinz M, Wu B, Jacobsen SE, Pollard JW, et al. A lineage of myeloid cells independent of Myb and hematopoietic stem cells. *Science*. 2012;336:86-90.

12. Yona S, Kim KW, Wolf Y, Mildner A, Varol D, Breker M, Strauss-Ayali D, Viukov S, Guilliams M, Misharin A, et al. Fate mapping reveals origins and dynamics of monocytes and tissue macrophages under homeostasis. *Immunity*. 2013;38:79-91.

13. Hashimoto D, Chow A, Noizat C, Teo P, Beasley MB, Leboeuf M, Becker CD, See P, Price J, Lucas D, et al. Tissue-resident macrophages self-maintain locally throughout adult life with minimal contribution from circulating monocytes. *Immunity*. 2013;38:792-804.

14. Epelman S, Lavine KJ, Beaudin AE, Sojka DK, Carrero JA, Calderon B, Brija T, Gautier EL, Ivanov S, Satpathy AT, et al. Embryonic and adult-derived resident cardiac macrophages are maintained through distinct mechanisms at steady state and during inflammation. *Immunity*. 2014;40:91-104.

15. Ensan S, Li A, Besla R, Degousee N, Cosme J, Roufaiel M, Shikatani EA, El-Maklizi M, Williams JW, Robins L, et al. Self-renewing resident arterial macrophages arise from embryonic CX3CR1(+) precursors and circulating monocytes immediately after birth. *Nat Immunol*. 2016;17:159-68.

16. Gomez Perdiguero E, Klapproth K, Schulz C, Busch K, Azzoni E, Crozet L, Garner H, Trouillet C, de Bruijn MF, Geissmann F, et al. Tissue-resident macrophages originate from yolk-sac-derived erythro-myeloid progenitors. *Nature*. 2015;518:547-51.

17. Bertrand JY, Jalil A, Klaine M, Jung S, Cumano A and Godin I. Three pathways to mature macrophages in the early mouse yolk sac. *Blood*. 2005;106:3004-11.

18. Hoeffel G and Ginhoux F. Fetal monocytes and the origins of tissue-resident macrophages. *Cell Immunol*. 2018;330:5-15.

19. Kasaai B, Caolo V, Peacock HM, Lehoux S, Gomez-Perdiguero E, Luttun A and Jones EA. Erythro-myeloid progenitors can differentiate from endothelial cells and modulate embryonic vascular remodeling. *Sci Rep*. 2017;7:43817.

20. Iturri L, Freyer L, Biton A, Dardenne P, Lallemand Y and Gomez Perdiguero E. Megakaryocyte production is sustained by direct differentiation from erythromyeloid progenitors in the yolk sac until midgestation. *Immunity*. 2021;54:1433-1446 e5.

21. Mass E, Ballesteros I, Farlik M, Halbritter F, Gunther P, Crozet L, Jacome-Galarza CE, Handler K, Klughammer J, Kobayashi Y, et al. Specification of tissue-resident macrophages during organogenesis. *Science*. 2016;353.

22. Palis J, Robertson S, Kennedy M, Wall C and Keller G. Development of erythroid and myeloid progenitors in the yolk sac and embryo proper of the mouse. *Development*. 1999;126:5073-84.

23. McGrath KE, Frame JM, Fegan KH, Bowen JR, Conway SJ, Catherman SC, Kingsley PD, Koniski AD and Palis J. Distinct Sources of Hematopoietic Progenitors Emerge before HSCs and Provide Functional Blood Cells in the Mammalian Embryo. *Cell Rep*. 2015;11:1892-904.

24. Stremmel C, Schuchert R, Wagner F, Thaler R, Weinberger T, Pick R, Mass E, Ishikawa-Ankerhold HC, Margraf A, Hutter S, et al. Yolk sac macrophage progenitors traffic to the embryo during defined stages of development. *Nat Commun*. 2018;9:75.

25. Hoeffel G, Chen J, Lavin Y, Low D, Almeida FF, See P, Beaudin AE, Lum J, Low I, Forsberg EC, et al. C-Myb(+) erythro-myeloid progenitor-derived fetal monocytes give rise to adult tissue-resident macrophages. *Immunity*. 2015;42:665-78.

26. Guilliams M, De Kleer I, Henri S, Post S, Vanhoutte L, De Prijck S, Deswarte K, Malissen B, Hammad H and Lambrecht BN. Alveolar macrophages develop from fetal monocytes that differentiate into long-lived cells in the first week of life via GM-CSF. *J Exp Med*. 2013;210:1977-92.

27. Sieweke MH and Allen JE. Beyond stem cells: self-renewal of differentiated macrophages. *Science*. 2013;342:1242974.

28. Plein A, Fantin A, Denti L, Pollard JW and Ruhrberg C. Erythro-myeloid progenitors contribute endothelial cells to blood vessels. *Nature*. 2018;562:223-228.

29. Feng T, Gao Z, Kou S, Huang X, Jiang Z, Lu Z, Meng J, Lin CP and Zhang H. No Evidence for Erythro-Myeloid Progenitor-Derived Vascular Endothelial Cells in Multiple Organs. *Circ Res*. 2020;127:1221-1232.

30. Murray PDF. The development in vitro of blood of early chick embryo. *Proc R Soc Lond Biol Sci*. 1932;111:497-521.

31. Zambidis ET, Park TS, Yu W, Tam A, Levine M, Yuan X, Pryzhkova M and Peault B. Expression of angiotensin-converting enzyme (CD143) identifies and regulates primitive hemangioblasts derived from human pluripotent stem cells. *Blood*. 2008;112:3601-14.

32. Takata K, Kozaki T, Lee CZW, Thion MS, Otsuka M, Lim S, Utami KH, Fidan K, Park DS, Malleret B, et al. Induced-Pluripotent-Stem-Cell-Derived Primitive Macrophages Provide a Platform for Modeling Tissue-Resident Macrophage Differentiation and Function. *Immunity*. 2017;47:183-198 e6.

33. Psaltis PJ and Simari RD. Vascular wall progenitor cells in health and disease. *Circ Res*. 2015;116:1392-412.

34. Psaltis PJ, Harbuzariu A, Delacroix S, Witt TA, Holroyd EW, Spoon DB, Hoffman SJ, Pan S, Kleppe LS, Mueske CS, et al. Identification of a monocyte-predisposed hierarchy of hematopoietic progenitor cells in the adventitia of postnatal murine aorta. *Circulation*. 2012;125:592-603.

35. Psaltis PJ, Puranik AS, Spoon DB, Chue CD, Hoffman SJ, Witt TA, Delacroix S, Kleppe LS, Mueske CS, Pan S, et al. Characterization of a resident population of adventitial macrophage progenitor cells in postnatal vasculature. *Circ Res*. 2014;115:364-75.

36. Weinberger T, Esfandyari D, Messerer D, Percin G, Schleifer C, Thaler R, Liu L, Stremmel C, Schneider V, Vagnozzi RJ, et al. Ontogeny of arterial macrophages defines their functions in homeostasis and inflammation. *Nat Commun*. 2020;11:4549.

37. Perdiguero EG, Klapproth K, Schulz C, Busch K, de Bruijn M, Rodewald HR and Geissmann F. The Origin of Tissue-Resident Macrophages: When an Erythro-myeloid Progenitor Is an Erythro-myeloid Progenitor. *Immunity*. 2015;43:1023-4.

38. Jung S, Aliberti J, Graemmel P, Sunshine MJ, Kreutzberg GW, Sher A and Littman DR. Analysis of fractalkine receptor CX(3)CR1 function by targeted deletion and green fluorescent protein reporter gene insertion. *Mol Cell Biol*. 2000;20:4106-14.

39. Dick SA, Macklin JA, Nejat S, Momen A, Clemente-Casares X, Althagafi MG, Chen J, Kantores C, Hosseinzadeh S, Aronoff L, et al. Self-renewing resident cardiac macrophages limit adverse remodeling following myocardial infarction. *Nat Immunol*. 2019;20:29-39.

40. Karsunky H, Merad M, Cozzio A, Weissman IL and Manz MG. Flt3 ligand regulates dendritic cell development from Flt3+ lymphoid and myeloid-committed progenitors to Flt3+ dendritic cells in vivo. *J Exp Med*. 2003;198:305-13.

41. Mass E, Ballesteros I, Farlik M, Halbritter F, Gunther P, Crozet L, Jacome-Galarza CE, Handler K, Klughammer J, Kobayashi Y, et al. Specification of tissue-resident macrophages during organogenesis. *Science*. 2016;353:aaf4238.

42. Kurotaki D, Sasaki H and Tamura T. Transcriptional control of monocyte and macrophage development. *Int Immunol*. 2017;29:97-107.

43. Nielsen JS and McNagny KM. CD34 is a key regulator of hematopoietic stem cell trafficking to bone marrow and mast cell progenitor trafficking in the periphery. *Microcirculation*. 2009;16:487-96.

44. Aziz A, Soucie E, Sarrazin S and Sieweke MH. MafB/c-Maf deficiency enables self-renewal of differentiated functional macrophages. *Science*. 2009;326:867-71.

45. Soucie EL, Weng Z, Geirsdottir L, Molawi K, Maurizio J, Fenouil R, Mossadegh-Keller N, Gimenez G, VanHille L, Beniazza M, et al. Lineage-specific enhancers activate self-renewal genes in macrophages and embryonic stem cells. *Science*. 2016;351:aad5510.

46. Greig KT, Carotta S and Nutt SL. Critical roles for c-Myb in hematopoietic progenitor cells. *Semin Immunol*. 2008;20:247-56.

47. Ribatti D. Genetic and epigenetic mechanisms in the early development of the vascular system. *J Anat*. 2006;208:139-52.

48. Iwatsuki K, Tanaka K, Kaneko T, Kazama R, Okamoto S, Nakayama Y, Ito Y, Satake M, Takahashi S, Miyajima A, et al. Runx1 promotes angiogenesis by downregulation of insulin-like growth factor-binding protein-3. *Oncogene*. 2005;24:1129-37.

49. Lukowski SW, Patel J, Andersen SB, Sim SL, Wong HY, Tay J, Winkler I, Powell JE and Khosrotehrani K. Single-Cell Transcriptional Profiling of Aortic Endothelium Identifies a Hierarchy from Endovascular Progenitors to Differentiated Cells. *Cell Rep*. 2019;27:2748-2758.e3.

50. Toledo-Flores D, Williamson A, Schwarz N, Fernando S, Dimasi C, Witt TA, Nguyen TM, Puranik AS, Chue CD, Delacroix S, et al. Vasculogenic properties of adventitial Sca-1(+)CD45(+) progenitor cells in mice: a potential source of vasa vasorum in atherosclerosis. *Sci Rep*. 2019;9:7286.

51. Patel J, Seppanen EJ, Rodero MP, Wong HY, Donovan P, Neufeld Z, Fisk NM, Francois M and Khosrotehrani K. Functional Definition of Progenitors Versus Mature Endothelial Cells Reveals Key SoxF-Dependent Differentiation Process. *Circulation*. 2017;135:786-805.

52. Lin C, Datta V, Okwan-Duodu D, Chen X, Fuchs S, Alsabeh R, Billet S, Bernstein KE and Shen XZ. Angiotensin-converting enzyme is required for normal myelopoiesis. *FASEB J*. 2011;25:1145-55.

53. Moore JP, Vinh A, Tuck KL, Sakkal S, Krishnan SM, Chan CT, Lieu M, Samuel CS, Diep H, Kemp-Harper BK, et al. M2 macrophage accumulation in the aortic wall during angiotensin II infusion in mice is associated with fibrosis, elastin loss, and elevated blood pressure. *Am J Physiol Heart Circ Physiol*. 2015;309:H906-17.

54. Rateri DL, Howatt DA, Moorleghen JJ, Charnigo R, Cassis LA and Daugherty A. Prolonged infusion of angiotensin II in apoE(-/-) mice promotes macrophage recruitment with continued expansion of abdominal aortic aneurysm. *Am J Pathol*. 2011;179:1542-8.

55. Satoh Y, Matsumura I, Tanaka H, Ezoe S, Sugahara H, Mizuki M, Shibayama H, Ishiko E, Ishiko J, Nakajima K, et al. Roles for c-Myc in self-renewal of hematopoietic stem cells. *J Biol Chem*. 2004;279:24986-93.

56. Li L, Jin H, Xu J, Shi Y and Wen Z. Irf8 regulates macrophage versus neutrophil fate during zebrafish primitive myelopoiesis. *Blood*. 2011;117:1359-69.

57. Wu J, Montaniel KR, Saleh MA, Xiao L, Chen W, Owens GK, Humphrey JD, Majesky MW, Paik DT, Hatzopoulos AK, et al. Origin of Matrix-Producing Cells That Contribute to Aortic Fibrosis in Hypertension. *Hypertension*. 2016;67:461-8.

58. Daugherty A, Manning MW and Cassis LA. Angiotensin II promotes atherosclerotic lesions and aneurysms in apolipoprotein E-deficient mice. *J Clin Invest*. 2000;105:1605-12.

59. Reu P, Khosravi A, Bernard S, Mold JE, Salehpour M, Alkass K, Perl S, Tisdale J, Possnert G, Druid H, et al. The Lifespan and Turnover of Microglia in the Human Brain. *Cell Rep*. 2017;20:779-784.

60. Huang Y, Xu Z, Xiong S, Sun F, Qin G, Hu G, Wang J, Zhao L, Liang YX, Wu T, et al. Repopulated microglia are solely derived from the proliferation of residual microglia after acute depletion. *Nat Neurosci*. 2018;21:530-540.

61. Ghigo C, Mondor I, Jorquera A, Nowak J, Wienert S, Zahner SP, Clausen BE, Luche H, Malissen B, Klauschen F, et al. Multicolor fate mapping of Langerhans cell homeostasis. *J Exp Med*. 2013;210:1657-64.

62. Tay TL, Mai D, Dautzenberg J, Fernandez-Klett F, Lin G, Sagar, Datta M, Drougard A, Stempfl T, Ardura-Fabregat A, et al. A new fate mapping system reveals context-dependent random or clonal expansion of microglia. *Nat Neurosci*. 2017;20:793-803.

63. Elmore MR, Najafi AR, Koike MA, Dagher NN, Spangenberg EE, Rice RA, Kitazawa M, Matusow B, Nguyen H, West BL, et al. Colony-stimulating factor 1 receptor signaling is necessary for microglia viability, unmasking a microglia progenitor cell in the adult brain. *Neuron*. 2014;82:380-97.

64. Auffray C, Fogg DK, Narni-Mancinelli E, Senechal B, Trouillet C, Saederup N, Leemput J, Bigot K, Campisi L, Abitbol M, et al. CX3CR1+ CD115+ CD135+ common macrophage/DC precursors and the role of CX3CR1 in their response to inflammation. *J Exp Med*. 2009;206:595-606.

65. Hettinger J, Richards DM, Hansson J, Barra MM, Joschko AC, Krijgsveld J and Feuerer M. Origin of monocytes and macrophages in a committed progenitor. *Nat Immunol*. 2013.

66. Samokhvalov IM, Samokhvalova NI and Nishikawa S. Cell tracing shows the contribution of the yolk sac to adult haematopoiesis. *Nature*. 2007;446:1056-61.

67. Potente M, Gerhardt H and Carmeliet P. Basic and therapeutic aspects of angiogenesis. *Cell*. 2011;146:873-87.

68. Manavski Y, Lucas T, Glaser SF, Dorsheimer L, Gunther S, Braun T, Rieger MA, Zeiher AM, Boon RA and Dimmeler S. Clonal Expansion of Endothelial Cells Contributes to Ischemia-Induced Neovascularization. *Circ Res*. 2018;122:670-677.

69. Asahara T, Masuda H, Takahashi T, Kalka C, Pastore C, Silver M, Kearne M, Magner M and Isner JM. Bone marrow origin of endothelial progenitor cells responsible for postnatal vasculogenesis in physiological and pathological neovascularization. *Circ Res*. 1999;85:221-8.

70. Kennedy M, D'Souza SL, Lynch-Kattman M, Schwantz S and Keller G. Development of the hemangioblast defines the onset of hematopoiesis in human ES cell differentiation cultures. *Blood*. 2007;109:2679-87.

71. Edgar R, Domrachev M and Lash AE. Gene Expression Omnibus: NCBI gene expression and hybridization array data repository. *Nucleic Acids Res*. 2002;30:207-10.

72. Bordt EA, Block CL, Petrozziello T, Sadri-Vakili G, Smith CJ, Edlow AG and Bilbo SD. Isolation of Microglia from Mouse or Human Tissue. *STAR Protoc*. 2020;1:100035.

73. Morgan K, Kharas M, Dzierzak E and Gilliland DG. Isolation of early hematopoietic stem cells from murine yolk sac and AGM. *J Vis Exp*. 2008:789.

74. McGinnis CS, Patterson DM, Winkler J, Conrad DN, Hein MY, Srivastava V, Hu JL, Murrow LM, Weissman JS, Werb Z, et al. MULTI-seq: sample multiplexing for single-cell RNA sequencing using lipid-tagged indices. *Nat Methods*. 2019;16:619-626.

75. Hao Y, Hao S, Andersen-Nissen E, Mauck WM, 3rd, Zheng S, Butler A, Lee MJ, Wilk AJ, Darby C, Zager M, et al. Integrated analysis of multimodal single-cell data. *Cell*. 2021;184:3573-3587.e29.

76. Yu G. Using ggtree to Visualize Data on Tree-Like Structures. *Curr Protoc Bioinformatics*. 2020;69:e96.

77. Trapnell C, Cacchiarelli D, Grimsby J, Pokharel P, Li S, Morse M, Lennon NJ, Livak KJ, Mikkelsen TS and Rinn JL. The dynamics and regulators of cell fate decisions are revealed by pseudotemporal ordering of single cells. *Nat Biotechnol*. 2014;32:381-386.

78. Qiu X, Hill A, Packer J, Lin D, Ma YA and Trapnell C. Single-cell mRNA quantification and differential analysis with Census. *Nat Methods*. 2017;14:309-315.

79. Qiu X, Mao Q, Tang Y, Wang L, Chawla R, Pliner HA and Trapnell C. Reversed graph embedding resolves complex single-cell trajectories. *Nat Methods*. 2017;14:979-982.

80. Wickham H. *ggplot2: Elegant Graphics for Data Analysis*: Springer-Verlag New York; 2016.

81. Percie du Sert N, Hurst V, Ahluwalia A, Alam S, Avey MT, Baker M, Browne WJ, Clark A, Cuthill IC, Dirnagl U, et al. The ARRIVE guidelines 2.0: updated guidelines for reporting animal research. *J Physiol*. 2020;598:3793-3801.

FIGURES AND FIGURE LEGENDS

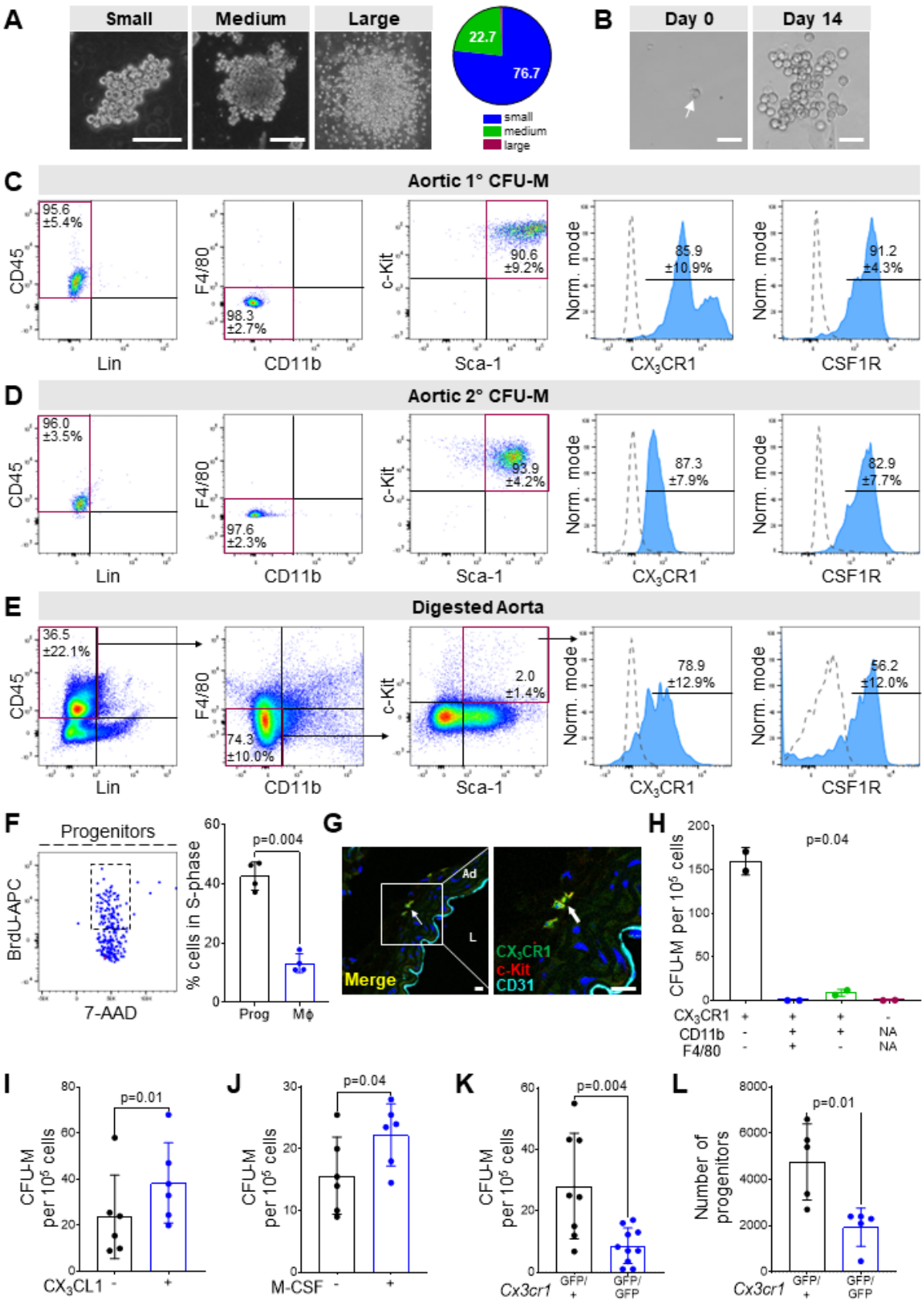

Figure 1. Immunophenotypic characterization of CFU-M progenitors in adult aorta.

(A) Examples of small, medium and large CFU-M from 12 w C57BL/6J aortic cells. Pie chart shows breakdown of CFU-M by colony size (n=5).

(B) Renewal of 2° CFU-M from a single cell plated from a medium 1° CFU-M.

(C, D) Flow cytometry of cells from (C) 1° and (D) 2° aortic CFU-M of medium size (n≥3 for each marker). Blue histogram, sample. Dotted histogram, Fluorescence-minus-one (FMO) control.

(E) Flow cytometry shows presence of progenitors in 12 w C57BL/6J aorta *in vivo* (n≥5 for each marker).

(F) Flow cytometry of bromodeoxyuridine (BrdU) uptake versus 7-aminoactinomycin (7-AAD) labeled cells gated from aortic progenitors *in vivo*. Dotted box, S-phase. Graph shows percentages of progenitors (Prog) and macrophages (Mϕ) in S-phase from 12 w C57BL/6J aorta 24 h after administration of BrdU (n=4). Paired t-test.

(G) Confocal microscopy of immunolabeled section of descending aorta from 12 w *Cx3cr1*$^{GFP/+}$ mouse shows adventitial (Ad) CX_3CR1^+c-Kit$^+$ progenitors. L, lumen.

(H) CFU-M yield from FACS-isolated cells from adult *Cx3cr1*$^{GFP/+}$ aortas (two experiments, n=6 mice each). N/A, not applicable.

(I, J) CFU-M yield from 12 w C57BL/6J aortic cells in presence of (I) 100 nM CX_3CL1 or (J) 50 nM M-CSF (n=6). Paired t-tests.

(K, L) Frequency of (K) CFU-M (n=8-10) and (L) progenitors (n=5) from aortas of 12 w *Cx3cr1*$^{GFP/+}$ and *Cx3cr1*$^{GFP/GFP}$ mice. Unpaired t-test for (K) and Mann-Whitney test for (L). Data summarized as mean±SD.

Scale bar, 100 µm in (A), (B) and 20 µm in (G).

Also see **Supplemental Figures S1-S3.**

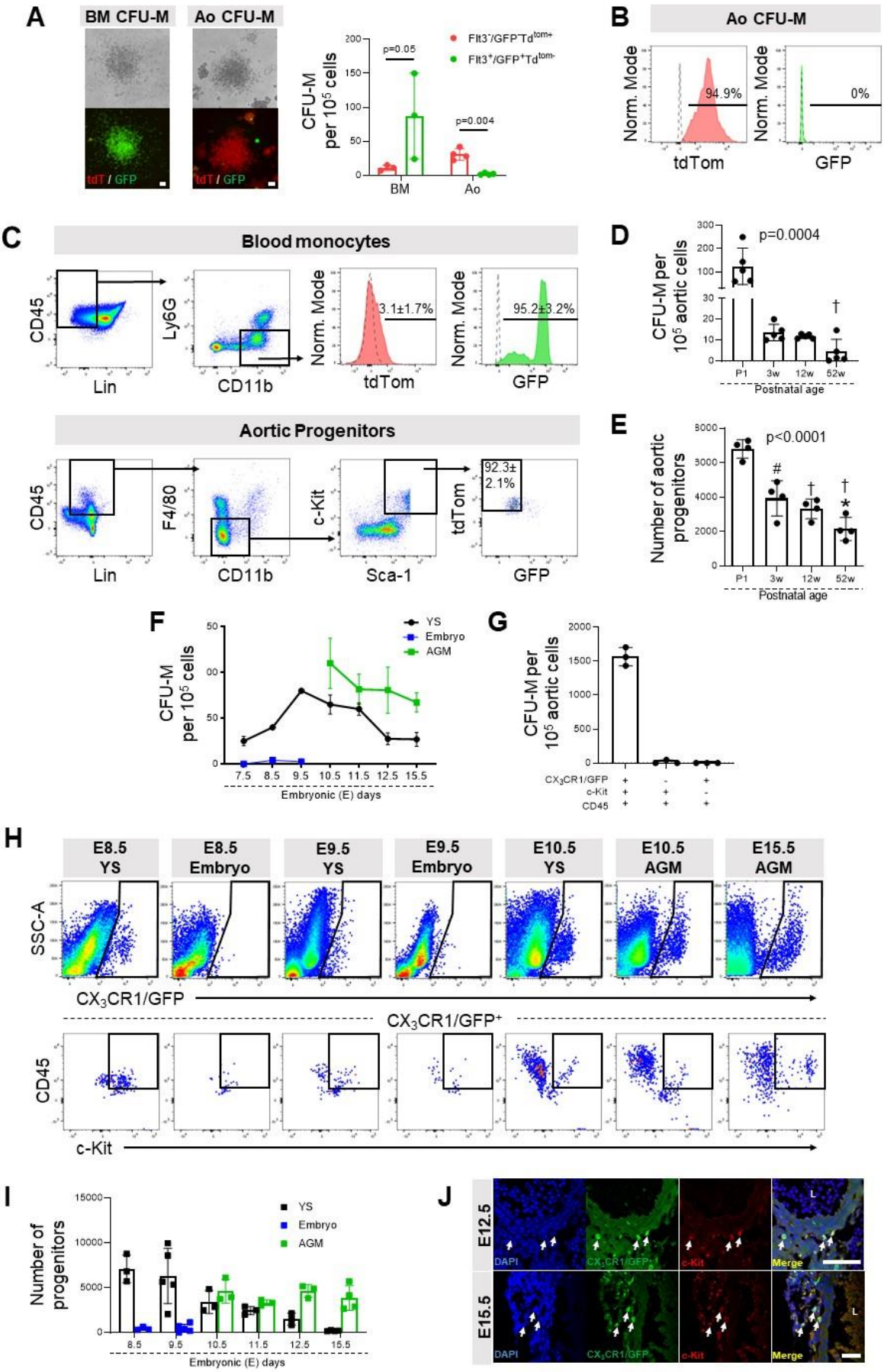

Figure 2. Aortic CFU-M progenitors are independent of Flt3⁺ hematopoiesis and are

seeded embryonically.

(A) Light and fluorescence microscopy images of CFU-M from BM and aorta (Ao) of adult *Flt3*^{Cre} x *Rosa*$^{mT/mG}$ mice. Graph shows Flt3^{+} (green) and Flt3^{-} (red) CFU-M yield from BM and Ao (n=3-4). Paired t-tests for each tissue.

(B) Flow cytometry histograms showing tdTom and GFP expression of cells in CFU-M from *Flt3*^{Cre} x *Rosa*$^{mT/mG}$ aorta (n=1). Dotted histogram, C57BL/6J control.

(C) Flow cytometry plots and histograms show tdTom^{+} (Flt3-cre^{-}) vs GFP^{+} (Flt3-cre^{+}) status of peripheral blood monocytes (n=6) and aortic progenitors (n=4) from adult *Flt3*^{Cre} x *Rosa*$^{mT/mG}$ mice. Percentages shown represent means. Dotted histograms, C57BL/6J control.

(D, E) Comparisons of (D) CFU-M yield (n=5; Kruskal-Wallis test) and (E) number of progenitors (n=4; One-way ANOVA) from C57BL/6J aortas at different ages. Multiple comparison tests: *p<0.05 for 3 w vs 52 w; †p<0.01 and #p<0.0001 for comparison to P1.

(F) CFU-M yield from different embryonic tissues of *Cx3cr1*$^{GFP/+}$ mice at different embryonic ages (n=1-12).

(G) CFU-M yield from different subpopulations of FACS-isolated cells from E9.5 YS from *Cx3cr1*$^{GFP/+}$ mice (n=3 experiments, each using ≥6 pooled YS). Repeated measures ANOVA p=0.003.

(H) Flow cytometry of digests of YS, whole embryo and AGM from *Cx3cr1*$^{GFP/+}$ mice at different embryonic ages showing CX$_3$CR1/GFP^{+} cells (top row) and CX$_3$CR1/GFP^{+}c-Kit^{+}CD45^{+} progenitors (bottom row) (n=3-5).

(I) Number of CX$_3$CR1/GFP^{+}c-Kit^{+}CD45^{+} progenitors in YS, whole embryo or AGM at different embryonic ages (n=3-5).

(J) Confocal microscopy of immunolabeled E12.5 and E15.5 AGM from *Cx3cr1*$^{GFP/+}$ mice shows adventitial CX$_3$CR1/GFP^{+}c-Kit^{+} progenitors (arrows). L, lumen.

Data summarized as mean or mean±SD.

Scale bar, 100 μm in (A) and 50 μm in (J).

Also see **Supplemental Figures S4** and S**5**.

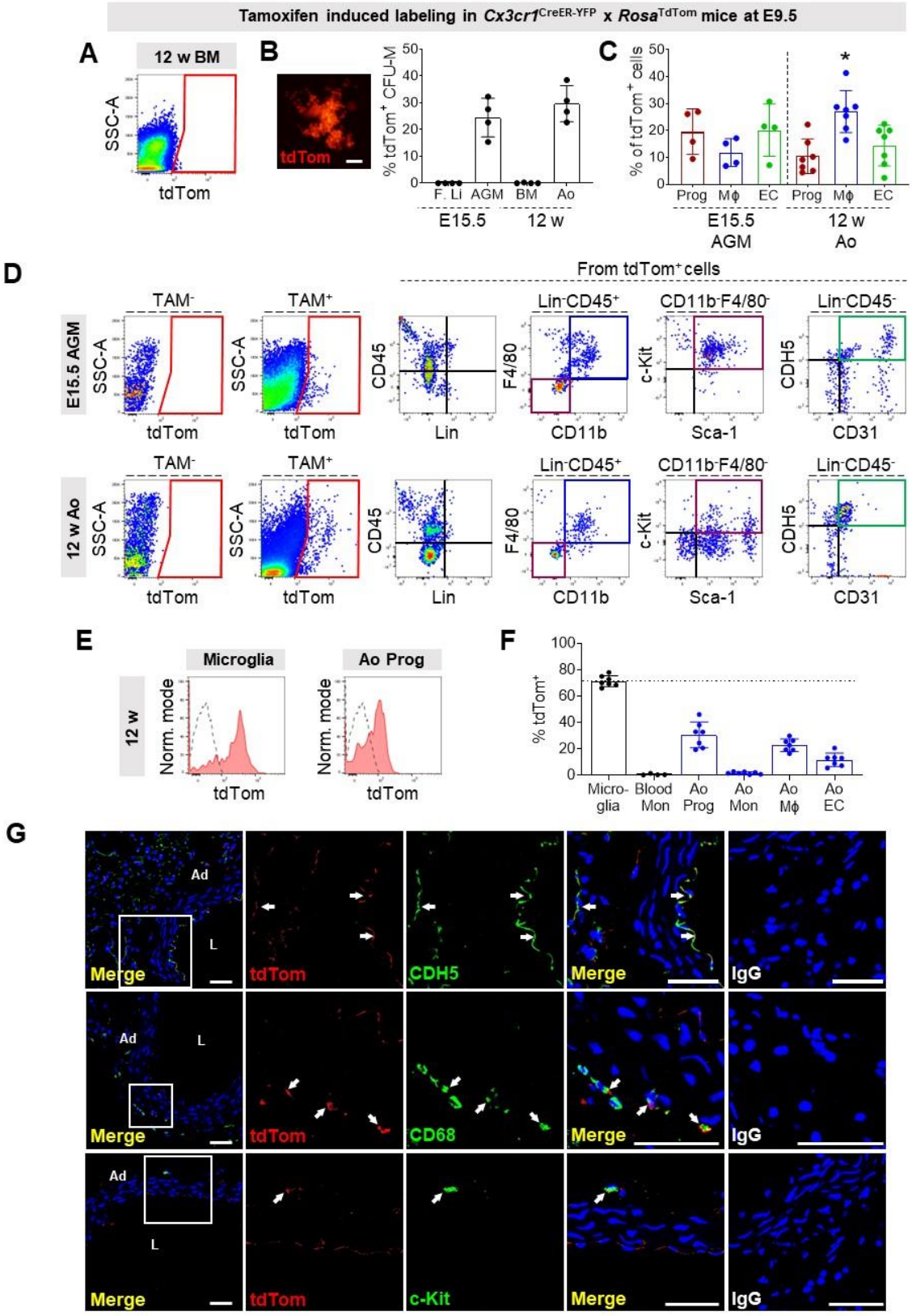

Figure 3. Aortic CFU-M progenitors arise from an early embryonic CX$_3$CR1$^+$ source.

(A-F) 4-hydroxytamoxifen (TAM)-induced labeling was performed in *Cx3cr1*$^{\text{CreER-YFP}}$ x *Rosa*^{tdTom} mice at E9.5 for subsequent analysis.

(A) Representative plot shows negligible tdTom expression in 12 w bone marrow (BM) (n=4).

(B) Image of tdTom^{+} CFU-M from 12 w aorta. Graph shows % of tdTom^{+} CFU-M from different tissues and ages (n=4). Ao, aorta. AGM, aorta-gonad-mesonephros. F.Li., fetal liver.

(C, D) Graph and flow cytometry plots show composition of tdTom^{+} cells in E15.5 AGM and 12 w aorta, with gated regions showing progenitors (Prog, maroon), macrophages (Mφ, blue) and endothelial cells (EC, green) (n=4-7). tdTom expression from *Cx3cr1*$^{\text{CreER-YFP}}$ x *Rosa*^{tdTom} mice which did not receive TAM is also shown as negative control. Repeated measures ANOVA p=0.004 for 12 w; Multiple comparison tests: *p<0.05 for Mφ vs Prog and EC.

(E, F) Histograms and graph show % tdTom expression in different populations from 12 w mice (n=4-7). Red histogram, sample. Dotted histogram, TAM negative control. Mon, monocytes.

(G) Confocal microscopy images of immunolabeled sections of adult aorta from E9.5 TAM-induced *Cx3cr1*$^{\text{CreER-YFP}}$ x *Rosa*^{tdTom} mice show VE-cadherin (top row), CD68 (middle row) and c-Kit (bottom row) expression in tdTom^{+} cells (arrows). Merged images of IgG controls for each labeling are also shown. Ad, adventitia. L, lumen.

Data summarized as mean±SD.

Scale bar, 100 μm in (B) and 40 μm in (G).

Also see **Supplemental Figure S6**.

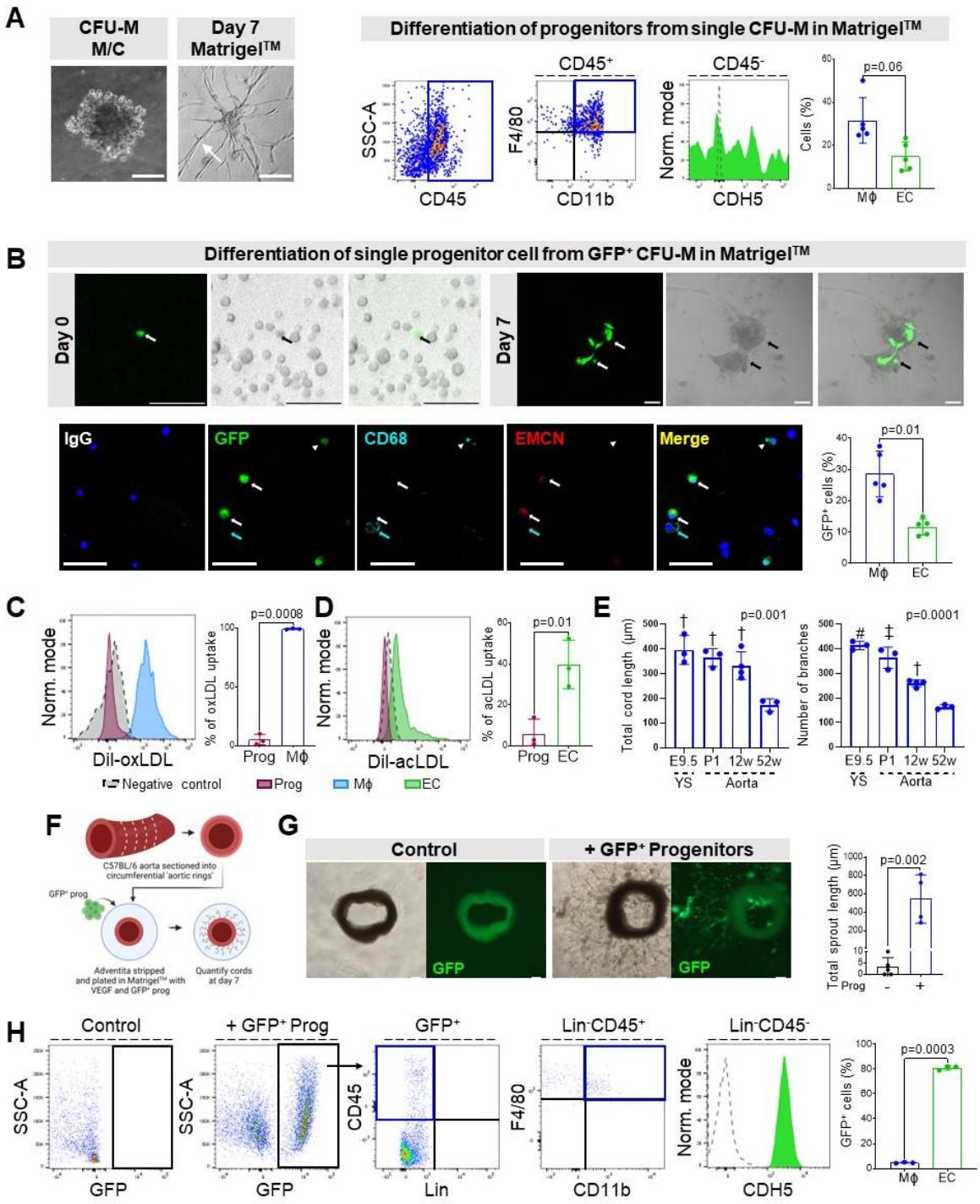

Figure 4. Aortic CFU-M progenitors have endothelial and macrophage potential.

(A) Light microscopy images show a single CFU-M from C57BL/6J aorta and the branching network formed by its progenitors in Matrigel™ after 7 d. Flow cytometry plots and graph show these networks contained new endothelial cells (EC) and macrophages (Mϕ) (n=5). Wilcoxon signed-rank test.

(B) Top row: Confocal microscopy images (fluorescence, phase contrast and merged) show single GFP^+ progenitor cell seeded with GFP^- progenitors at day 0 and the resulting GFP^+ sprout at day 7. Bottom row: Confocal microscopy images of immunolabeled cells show presence of GFP^+CD68^+ macrophage (arrowhead) and GFP^+EMCN^+ endothelial cells (white arrows). Cyan arrow indicates GFP^-CD68^+ macrophage. Merged image from corresponding IgG isotype negative control staining is also shown. Graph summarises frequency of macrophages and endothelial cells arising from a single GFP^+ progenitor cell in replicate wells containing both cell types (n=5). Paired t-test.

(C, D) Uptake of (C) DiI-oxLDL or (D) DiI-acLDL by aortic progenitors and their macrophage or endothelial cell progeny produced in Matrigel™ (n=3). Paired t-tests.

(E) Total cord length and number of branches produced in Matrigel™ by E9.5 YS or aortic CFU-M progenitors from C57BL/6J mice of different ages (n=3-4). One-way ANOVA. Multiple test comparisons: †$p<0.01$, ‡$p<0.001$ and #$p<0.0001$ for comparison to 52 w.

(F) Schematic of adventitial sprouting assay performed by culturing aortic progenitors from adult GFP mice with adventitia-less aortic rings from adult C57BL/6J mice.

(G) Light and fluorescence microscopy images show adventitial sprouting without (control) and with (+) addition of GFP^+ aortic progenitors and graph summarizes the results (n=4-5). Unpaired t-test.

(H) Flow cytometry plots and graph show the cells produced by culturing GFP^+ aortic progenitors in aortic ring assay for 7 d (n=3). Paired t-test.

Data summarized as mean±SD. Scale bar, 100 µm.

Also see **Supplemental Figure S8** and **S9** and **Supplemental Table S1**.

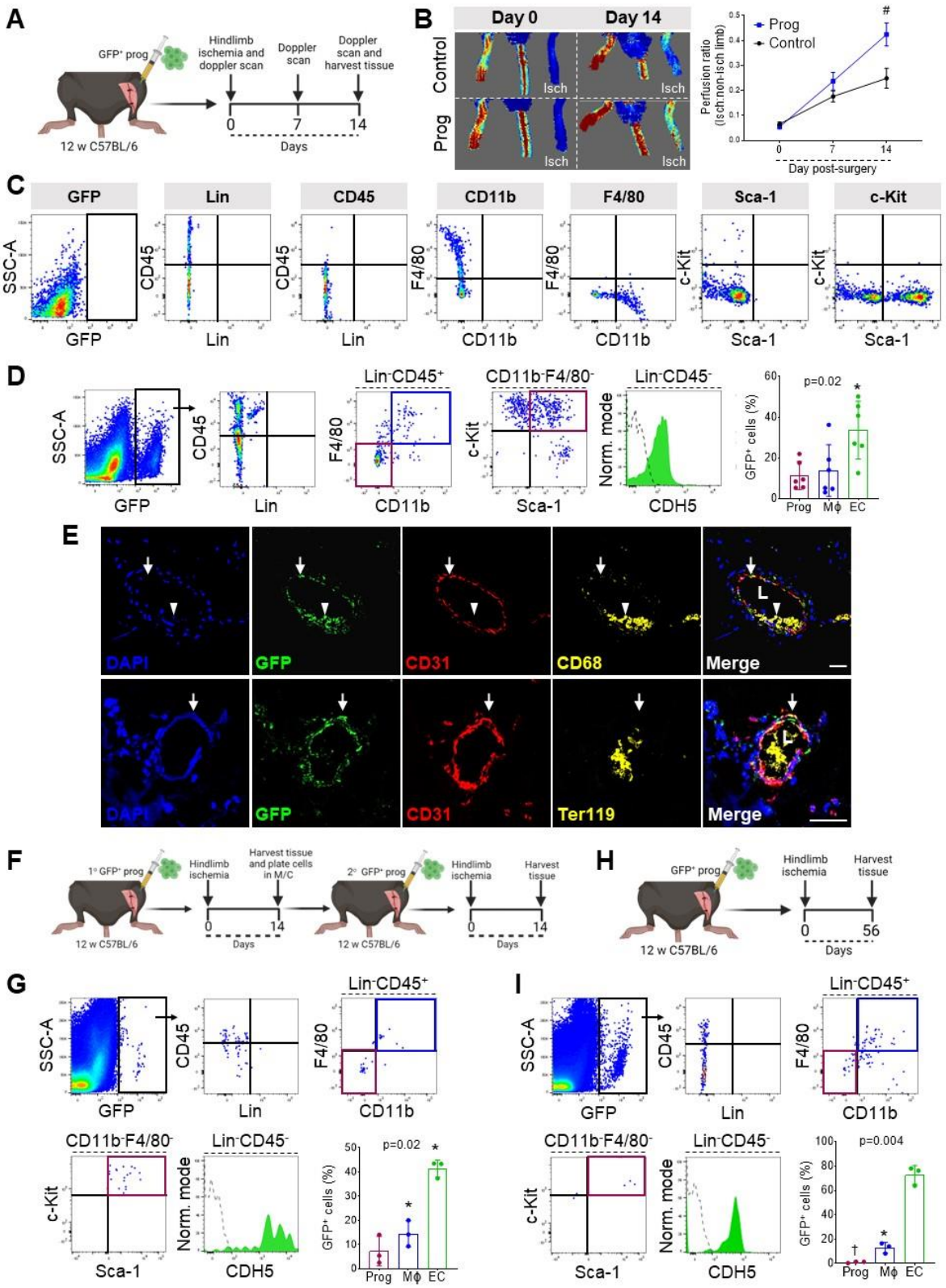

Figure 5. CFU-M progenitors have endothelial-macrophage plasticity and vasculogenic capacity *in vivo*.

(A) Schematic of 1º transfer of GFP$^+$ aortic progenitors in hindlimb muscle after hindlimb

ischemia surgery with two-week follow-up.

(B) Laser Doppler perfusion images of mice on day 0 and 14 after ischemia surgery and receiving cell-free control (above) or progenitors (below). Graph shows results over time (n=6/gp). Mixed effects two-way ANOVA: $p<0.0001$ for time; $p=0.03$ for group; $p=0.005$ for time x group. Multiple comparison test: #$p<0.0001$ for progenitors vs control.

(C) FMO control staining used to analyze the composition of cells produced by engrafted GFP^+ progenitors after transfer into ischemic hindlimb muscle.

(D) Flow cytometry plots and graph show the cells produced by donor cells in recipient muscle (n=6). Green histogram, sample; dotted histogram, FMO control. Repeated measures ANOVA. Multiple comparison test: *$p<0.05$ vs macrophages.

(E) Confocal microscopy of immunolabeled recipient ischemic muscle shows neovessels lined by GFP^+CD31^+ endothelial cells (arrows) with cluster of GFP^+CD68^+ macrophages (arrowhead) (above) and perfused with host TER-119^+ erythrocytes (below). L, lumen.

(F) Schematic of 2° transfer of GFP^+ progenitors into hindlimb muscle after hindlimb ischemia surgery.

(G) Flow cytometry plots and graph show cells produced by donor cells after 2° transfer (n=3). Repeated measures ANOVA. Multiple comparison test: *$p<0.05$ vs progenitors.

(H) Schematic of 1° transfer of GFP^+ aortic progenitors in hindlimb muscle after induction of hindlimb ischemia with 8 w follow-up.

(I) Flow cytometry plots and graph show cells produced by donor cells 8 w after 1° transfer (n=3). Repeated measures ANOVA. Multiple comparison test: *$p<0.05$ and †$p<0.01$ vs endothelial cells.

Data summarized as mean±SD.

Scale bar, 20 µm. Also see **Supplemental Figure S10**.

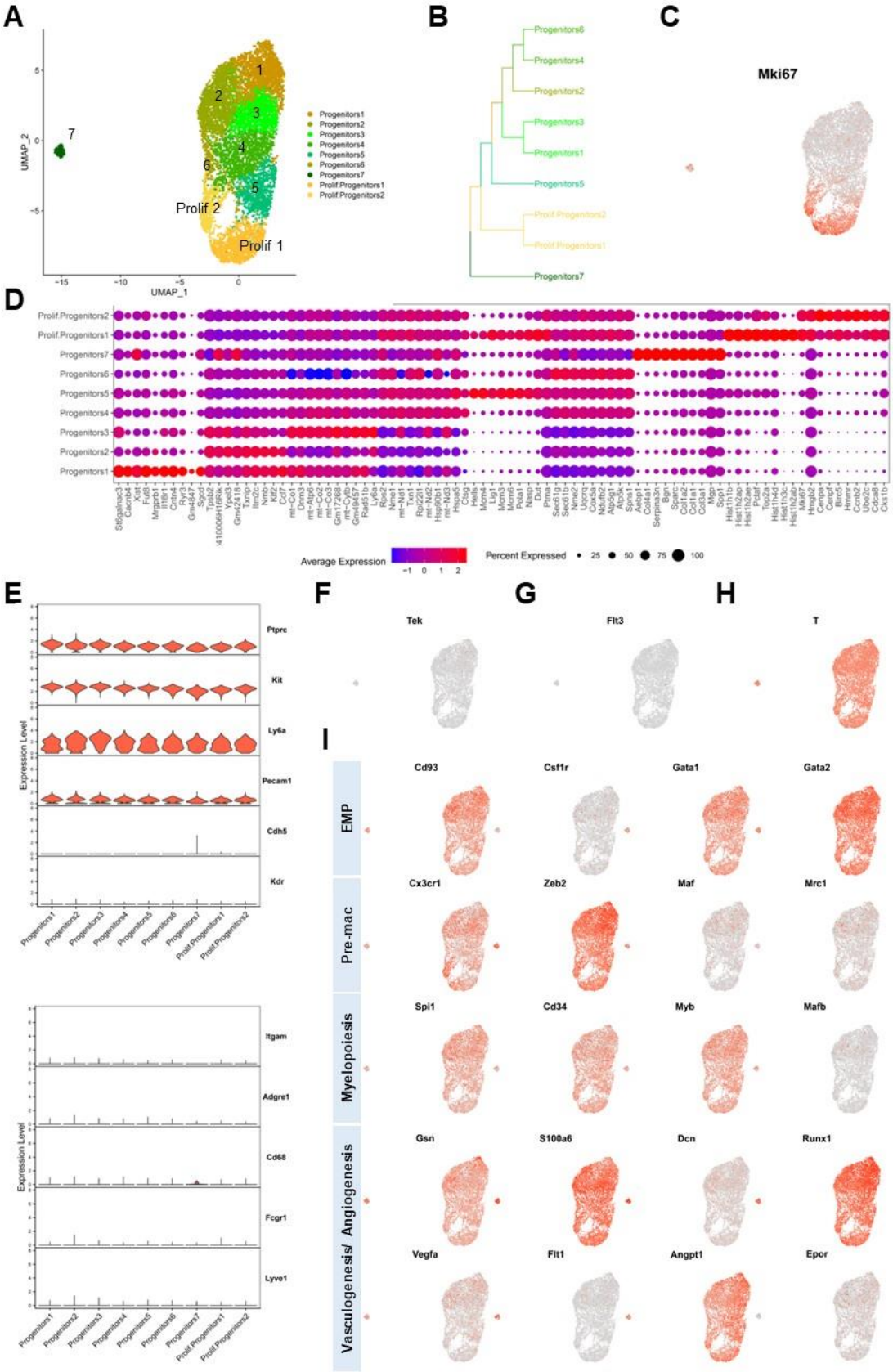

Figure 6. Aortic CFU-M progenitors exhibit a myelopoietic and vasculogenic transcriptional profile.

Aortic CFU-M progenitors cultured from two adult C57BL/6J mice were pooled and viable cells analyzed by scRNA-seq.

(A) UMAP plot of 7,966 cells that passed quality controls colored by cluster assignment. Each dot represents a cell. Cell clusters are colored as indicated.

(B) Phylogenetic tree shows the hierarchical relationships of assigned clusters.

(C) Expression levels of *Mki67* overlaid on the UMAP plot showing cell specificity of expression. Expression levels are shown as log normalized counts. The gray to red gradient represents low to high values. Predominant expression can be seen in the proliferative clusters.

(D) Dot plot shows the top 10 differentially expressed genes in each cluster and relative expression levels of those genes in all clusters. Purple to red gradient represents average expression levels from low to high. Dot size denotes percentage of cells expressing a gene, as indicated.

(E) Violin plots illustrate cluster-wise expression of the genes corresponding to the key surface markers expressed by progenitors, along with selected mature endothelial (top) and macrophage marker (bottom) genes.

F) Expression levels of the endothelial gene *Tek* overlaid on the UMAP plot showing minimal expression.

(G-I) Expression levels of the indicated marker genes for G) definitive hematopoiesis, H) hemangioblasts from embryonic mesenchyme, I) YS EMPs (EMP), pre-macrophages (Pre-mac), myelopoiesis and vasculogenesis/angiogenesis, overlaid on the UMAP plot showing cell specificity of expression.

Also see **Supplemental Figure S11**.

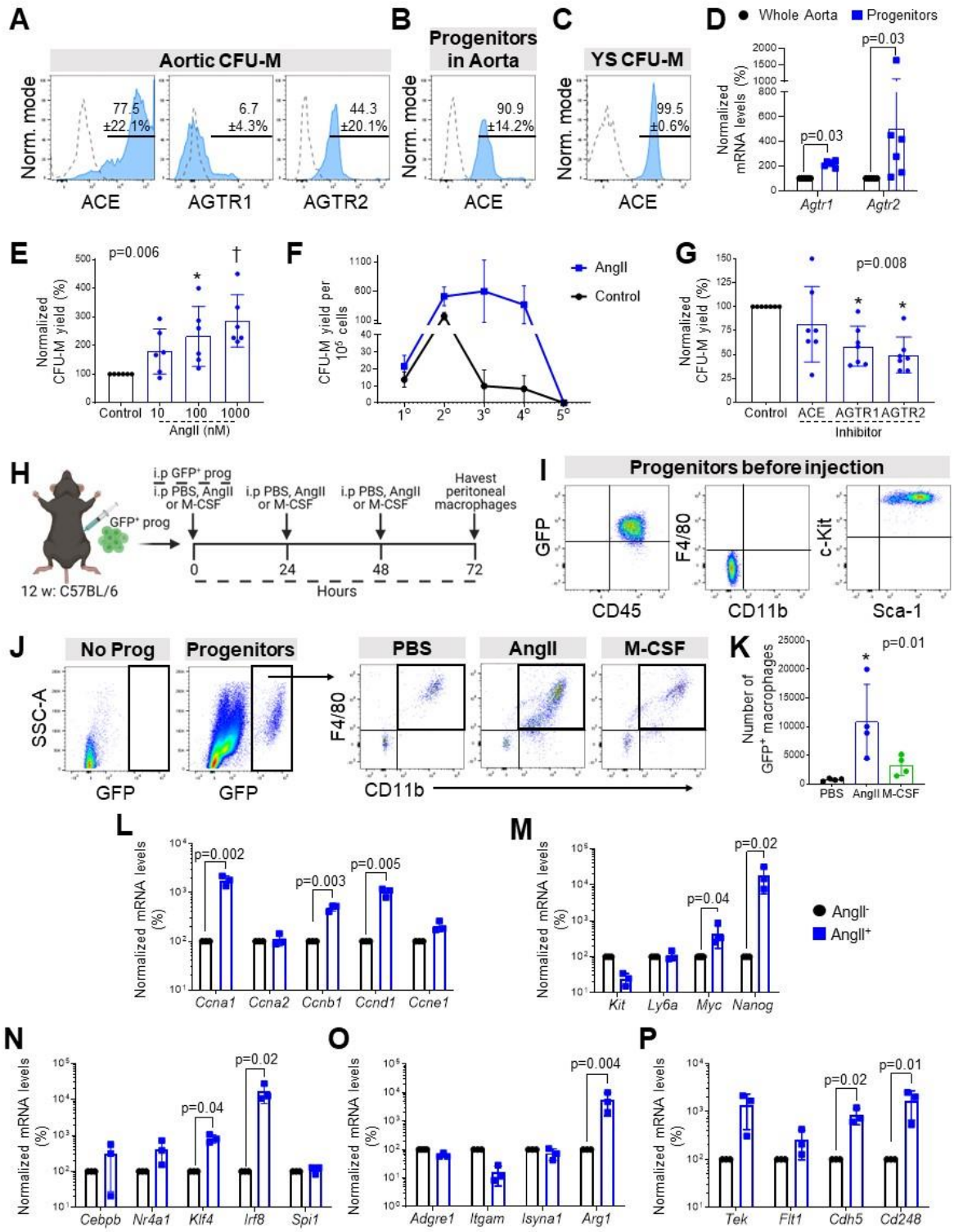

Figure 7. Regulatory effects of Angiotensin II on aortic EndoMac progenitors.

(A) Surface expression of ACE, AGTR1 and AGTR2 on progenitors from aortic CFU-M (n=5-6 12 w C57BL/6J mice).

(B) ACE expression on progenitors in 12 w C57BL/6J aortic digests (n=4).

(C) ACE expression on progenitors from E9.5 C57BL/6J YS CFU-M (n=3).

(D) Normalized mRNA expression of *Agtr1* and *Agtr2* in progenitors from aortic CFU-M relative to donor-matched aortic digests (n=6 12w C57BL/6J mice). Wilcoxon signed-rank tests.

(E) Aortic CFU-M yield with different concentrations of AngII, normalized to no AngII control (n=6 12 w C57BL/6J mice). Friedman test. Multiple comparison tests: *$p<0.05$, †$p<0.01$ vs control.

(F) Aortic CFU-M yield across serial passages in the presence or absence of 100 nM AngII (n=3-4 12 w C57BL/6J mice).

(G) Aortic CFU-M yield in the presence of inhibitors of ACE (Enalapril), AGTR1 (Losartan) and AGTR2 (PD123319) normalized to no inhibitor control (n=7). Friedman test. Multiple comparison tests: *$p<0.05$ vs control.

(H) Schematic of peritoneal transfer assay. GFP^+ aortic progenitors were intraperitoneally injected into 12 w C57BL/6J mice with daily injections of PBS, AngII or M-CSF for 72 h.

(I) Immunophenotype of GFP^+ aortic progenitors before intraperitoneal injection.

(J) Flow cytometry shows *de novo* formation of macrophages from GFP^+ aortic progenitors in peritoneal cavity after 72 h. No progenitor cells (Prog) negative control for GFP also shown.

(K) Number of macrophages produced by progenitors under different conditions (n=4). One-way ANOVA. Multiple comparisons test: *$p<0.05$ vs PBS.

(L-P) mRNA expression of selected genes in aortic progenitors after treatment with AngII. Expression normalized to *β-actin* and then no AngII control. Genes relate to (L) cell cycle; (M) progenitor/stem cell biology and self-renewal; (N) myelopoiesis; (O) macrophages; (P) endothelial biology and angiogenesis (n=3 12 w C57BL/6J mice). Paired t-tests.

Data summarized as mean±SD.

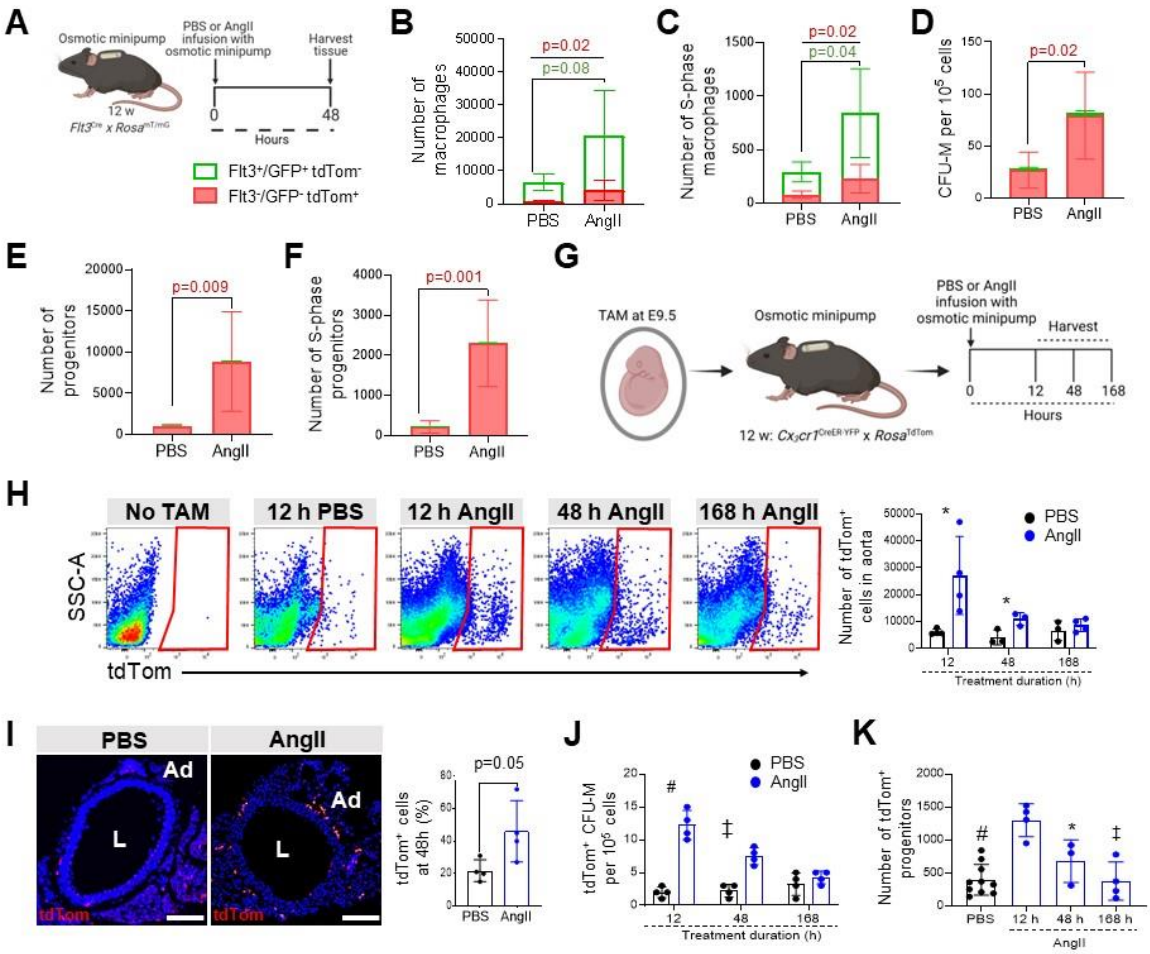

Figure 8. Angiotensin II-induced vascular inflammation involves early expansion of EndoMac progenitors *in vivo*.

(A) Schematic of PBS or AngII infusion in adult *Flt3*^{Cre} x *Rosa*$^{mT/mG}$ mice for 48 h.

(B-F) Comparisons of aortas from PBS and AngII groups for the numbers of Flt3-cre^{+} (green) and Flt3-cre^{-} (red): (B) macrophages, (C) S-phase macrophages, (D) CFU-M yield, (E) progenitors and (F) S-phase progenitors (n=5-6/gp). Flow cytometry used for (B), (C), (E) and (F). Unpaired t-tests. P-values in red, Flt3-cre^{-} comparisons; in green, Flt3-cre^{+} comparisons.

(G) Schematic of PBS or AngII infusion in E9.5 TAM-induced 12 w *Cx3cr1*$^{CreER\text{-}YFP}$ x *Rosa*^{tdTom} mice with aortas harvested at different times.

(H) Flow cytometry of tdTom^{+} labeling in aortic digests at different times. No TAM control also shown. Graph summarizes number of tdTom^{+} cells in aortas (n=3-4). Two-way ANOVA:

Interaction p=0.04, Time p=0.005, Group p=0.03. Mann-Whitney or unpaired t-tests also used to compare groups for each time point: *p<0.05.

(I) Confocal microscopy of immunolabeled sections of descending aorta after 48 h of PBS or AngII. Graph shows % of $tdTom^+$ cells in adventitia (Ad) (n=4, three sections each). Unpaired t-test. L, lumen. Nuclei stained with DAPI (blue).

(J) $tdTom^+$ aortic CFU-M yield (n=4). Two-way ANOVA: Interaction p<0.0001, Time p=0.0005, Group p<0.0001. Unpaired t-tests also used to compare groups for each time point: #p<0.0001, ‡p<0.001.

(K) Numbers of $tdTom^+$ progenitors in aorta after different durations of AngII or PBS (n=3-10). One-way ANOVA p=0.0001. Multiple comparisons test: *p<0.05, ‡p<0.001, #p<0.0001 vs 12 h.

Data summarized as mean±SD. Scale bar, 50 μm.

SUPPLEMENTAL TABLES

Supplemental Table S1. Sub-lineage marker expression of cells produced by aortic EndoMac progenitors in different experimental models.

Experimental Design	**Matrigel™** ***In vitro*** **N=3-6**	**Aortic Ring** ***Ex vivo*** **N=2-3**	**Hindlimb** ***In vivo*** **N=3-6**
Surface marker	**$CD45^+CD11b^+F4/80^+$ Macrophages**		
$CD206^+$	75.8 ± 23.9%	85.1 ± 20.6%	68.4 ± 17.0%
CX_3CR1^+	74.5 ± 16.3%	90.9 ± 13.4%	91.0 ± 8.7%
MHC II^+	5.8 ± 2.5%	2.9 ± 0.0%	19.4 ± 7.2%
LYVE-1^+	45.0 ± 21.4%	83.9 ± 0.8%	61.2 ± 16.5%
$CCR2^+$	5.5 ± 4.1%	ND	27.6 ±1.9%
	$CD45^-CD31^+$ and/or $CD45^-CDH5^+$ Endothelial cells		
$VEGFR2^+$	40.0 ± 13.3%	23.6 ± 0.8%	77.9 ± 19.4%
$TIE2^+$	80.4 ± 3.9%	ND	ND

Expression of select surface markers on macrophages and endothelial cells produced by adult aortic progenitors in Matrigel™ cord-forming assay, aortic ring assay and after intramuscular injection in hindlimb ischemia model. N-values relate to number of different experiments in which these markers were assessed. ND, not determined. Results are summarized as mean ± standard deviation. Also see **Figure 4, 5** and **Supplemental Figure S8, S10**.

Supplemental Table S2. Cell Ranger summary statistics for scRNA-seq runs.

	Sequencing run 1	Sequencing run 2	Combined output from two runs
Estimated Number of Cells	29,539	32,789	34,813
Mean Reads per Cell	14,912	48,013	54,874
Median Genes per Cell	2,306	3,427	3,534
Number of reads	440,473,799	1,574,282,809	2,014,756,608
Sequencing saturation	25.3%	54.5%	60.3%
Fraction reads in cell	90.2%	93.1%	95.2%
Total genes detected	25,482	26,164	26,617
Median UMI counts per cell	6,399	12,426	13,116

Two sequencing runs were performed to achieve ~50,000 mean reads per cell.

Supplemental Table S3. Numbers of cells contained within aortic CFU-M progenitor cell clusters identified by scRNA-seq.

Cell cluster	Number of cells
Progenitors1	1,558
Progenitors2	1,510
Progenitors3	1,130
Progenitors4	1,126
Progenitors5	775
Progenitors6	262
Progenitors7	133
Prolif.Progenitors1	950
Prolif.Progenitors2	522

Please see Supplemental Tables S4-S16 in the Excel file "Supplemental Material Tables S4-S16".

SUPPLEMENTAL FIGURES

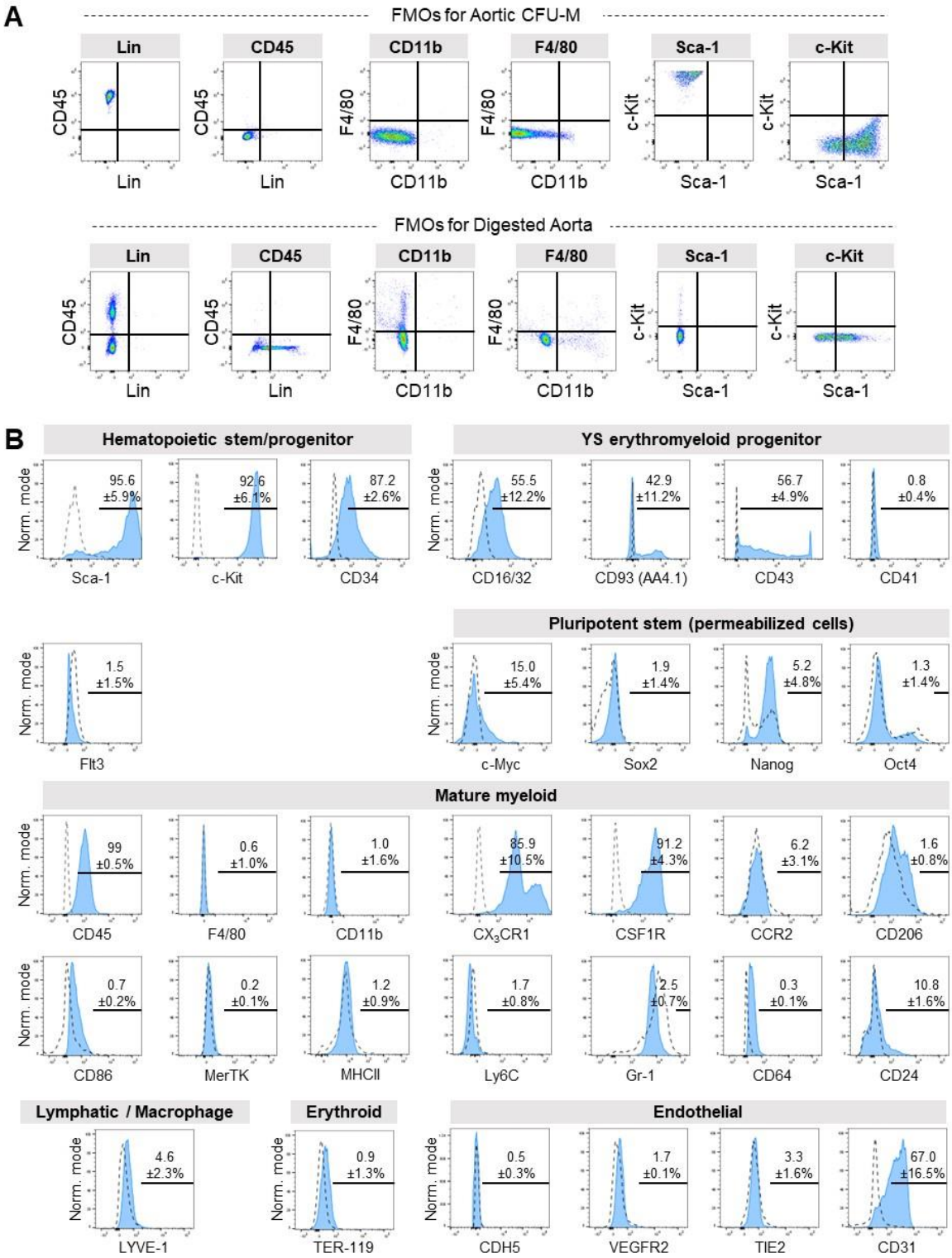

Supplemental Figure S1. Surface marker expression of progenitors contained within 1° aortic CFU-M.

(A) Top row: Fluorescence-minus-one (FMO) controls for flow cytometry performed on cells from medium-sized aortic CFU-M in **Figure 1C** and **D**. Bottom row: FMO controls used for flow cytometry performed on cells from aortic digests in **Figure 1E**.

(B) Flow cytometry histograms show expression of different surface markers on cells from medium-sized 1° aortic CFU-M (blue histogram). Dotted histogram, FMO control. Mean±SD % expression values are shown from n≥3 12 w C57BL/6J mice.

Also see **Figure 1**.

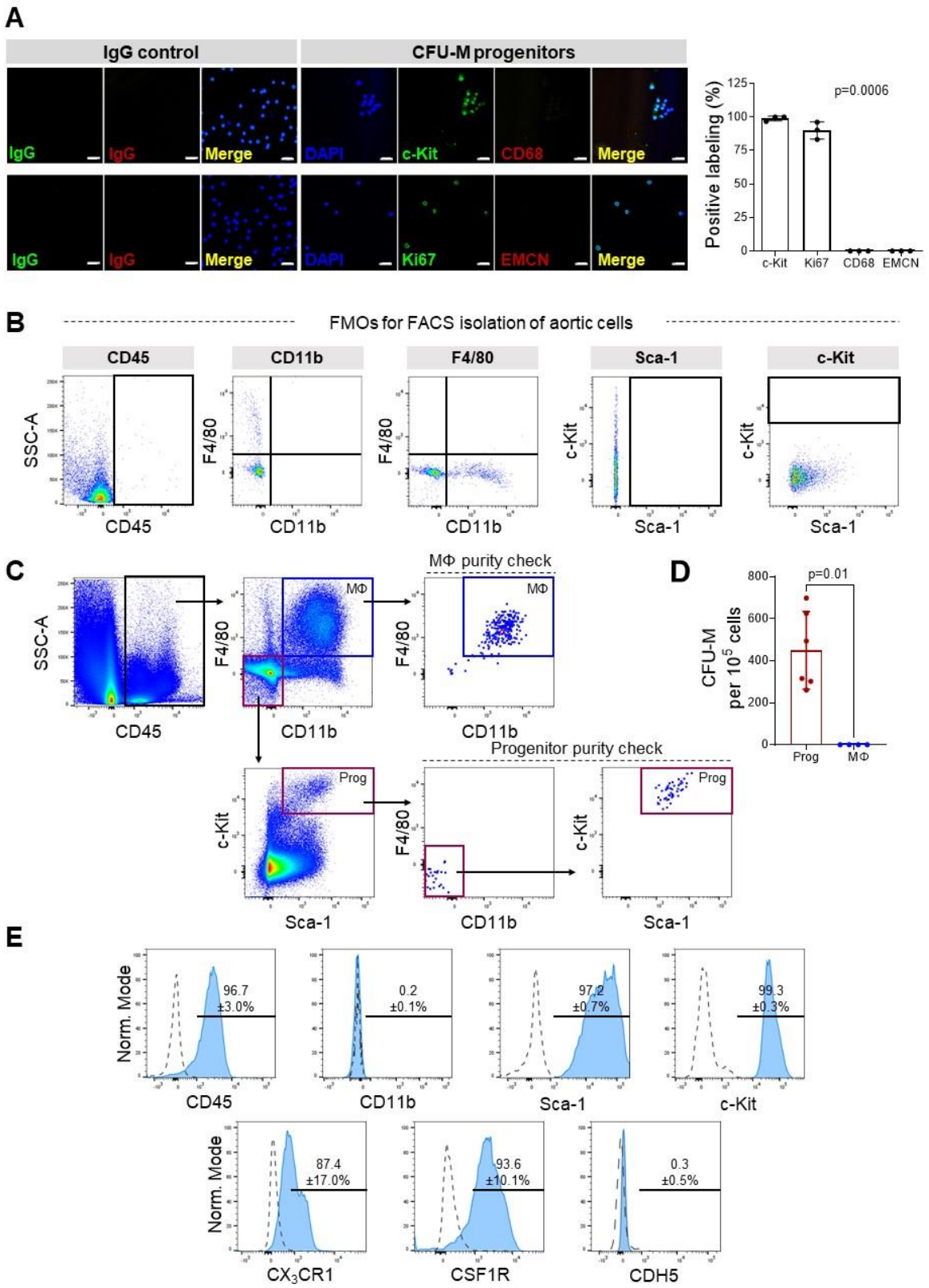

Supplemental Figure S2. Immunophenotypic confirmation of cell population responsible for aortic CFU-M.

(A) Confocal microscopy images of immunofluorescence labeling of cytospin preparations of

cells from aortic CFU-M. Scale bar, 100µm. Graph summarizes % of positively labeled cells with each marker. Data from three separate experiments using CFU-M from adult C57BL/6J aorta. Kruskal-Wallis test.

(B) FMO controls used for FACS to isolate progenitors (Prog) and macrophages (MΦ) from aortic cells of adult C57BL/6J mice.

(C) Representative flow cytometry dot plots used to FACS isolate progenitors and macrophages from aorta, with purity checks of sorted populations.

(D) Graph summarizes CFU-M yield from sorted aortic cell populations. N=4-6 independent experiments each using aortas from ≥6 mice. Mann-Whitney test.

(E) Flow cytometry histograms showing surface marker expression of cells contained in CFU-M produced by sorted aortic progenitors (blue). Dotted histograms, FMO controls. N=3. Data summarized as mean±SD.

Also see **Figure 1**.

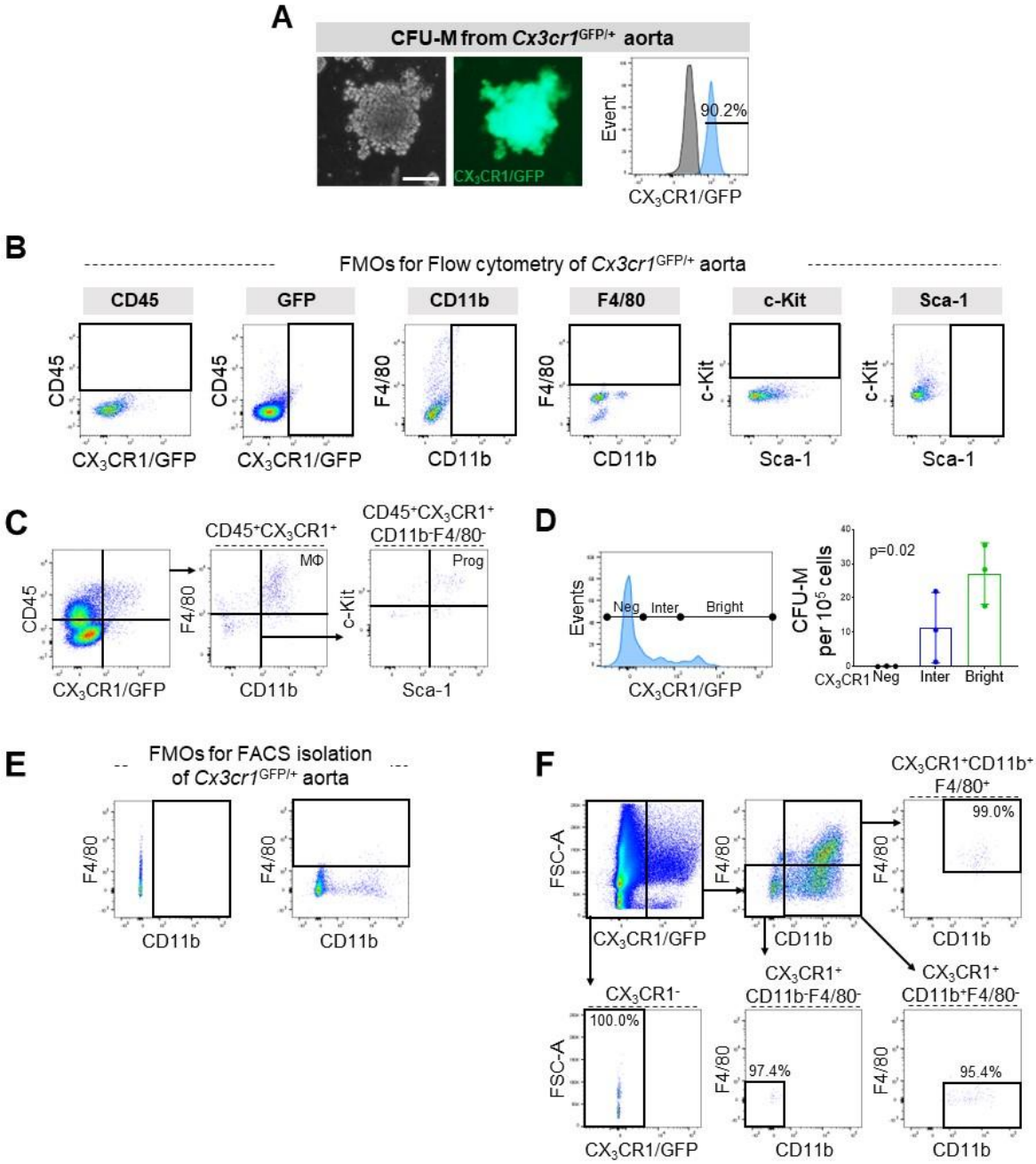

Supplemental Figure S3. Aortic CFU-M progenitors express CX_3CR1.

(A) Light and fluorescence microscopy and flow cytometry (blue histogram) show GFP^+ (CX_3CR1^+) expression of cells contained in CFU-M from 12 w *Cx3cr1*$^{GFP/+}$ aortas. Gray histogram, C57BL/6J control. N=1. Scale bar, 100 µm.

(B) FMO controls used for flow cytometry analysis of aortic digests from *Cx3cr1*$^{GFP/+}$ mice.

(C) Flow cytometry shows presence of $CD11b^-F4/80^-Sca\text{-}1^+c\text{-}Kit^+$ progenitors and $CD11b^+F4/80^+$ macrophages among $CD45^+CX_3CR1^+$ cells in aortas of 12 w *Cx3cr1*$^{GFP/+}$

mice. Representative of N=6.

(D) FACS isolation of CX_3CR1^{Neg}, CX_3CR1^{Inter} and CX_3CR1^{Bright} populations from 12 w *Cx3cr1*$^{GFP/+}$ aortas. Graph shows 1° CFU-M yield from each population (three experiments, six aortas each). Repeated measures one-way ANOVA.

(E) FMO controls used for FACS isolation of aortic cells from *Cx3cr1*$^{GFP/+}$ mice.

(F) Gating strategy and purity checks for FACS isolation of aortic cells from 12 w *Cx3cr1*$^{GFP/+}$ mice into $CX_3CR1^{+}CD11b^{-}F4/80^{-}$, $CX_3CR1^{+}CD11b^{+}F4/80^{+}$, $CX_3CR1^{+}CD11b^{+}F4/80^{-}$ and CX_3CR1^{-} populations, used in **Figure 1H**.

Data summarized as mean±SD.

Also see **Figure 1**.

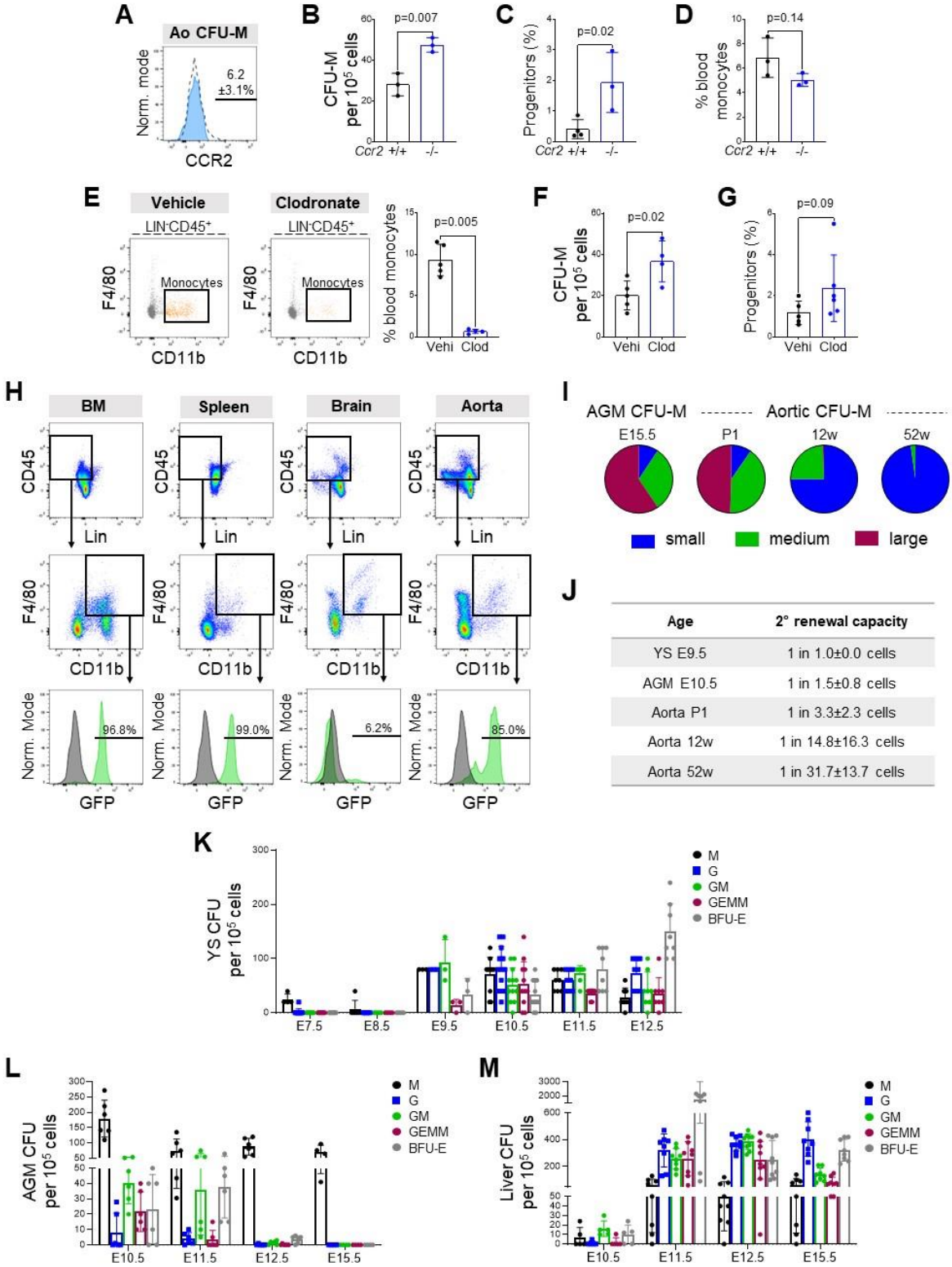

Supplemental Figure S4. Origins of aortic CFU-M progenitors.

(A) Surface expression of CCR2 on progenitor cells from 1° aortic CFU-M (blue histogram). Dotted histogram, FMO control. N=3.

(B-D) Graphs show comparisons of (B) CFU-M yield and (C) percentage of progenitors in

aorta, and (D) blood monocytes between 12 w *Ccr2*$^{+/+}$ and *Ccr2*$^{-/-}$ mice, measured by flow cytometry. N=3. Unpaired t-tests.

(E-G) Flow cytometry plots and graphs showing comparisons of (E) percentage of blood monocytes, and (F) CFU-M yield and (G) percentage of progenitors in aorta of 12 w C57BL/6J mice following treatment with clodronate (Clod) or vehicle (Vehi). N=4-6. Unpaired t-tests for (E) and (F) and Mann-Whitney test for (G).

(H) Flow cytometry of GFP^{+} (Flt3-Cre^{+}) expression on macrophages from different tissues of adult *Flt3*^{Cre} x *Rosa*^{mTmG} mice. Green histogram, sample. Gray histogram, control. Percentages shown are mean % GFP^{+} cells from N=3-4 mice.

(I) Pie charts show classification of CFU-M based on colony size from E15.5 AGM and aorta at different postnatal ages from C57BL/6J mice. N=3-6 mice per age.

(J) Frequency of self-renewal of progenitor cells from 1° CFU-M from YS, AGM and aorta at different ages, expressed as the number of individually seeded cells required to generate a 2° CFU-M. N=3-20 replicates per age.

(K-M) Frequency of different CFU types from (K) YS, (L) AGM and (M) liver at different embryonic ages. N=1-6 C57BL/6J embryos per gestational age. M, macrophage; GM, granulocyte-macrophage; GEMM, granulocyte-erythrocyte-monocyte-megakaryocyte; G, granulocyte; BFU-E, burst-forming units-erythroid.

Data summarized as mean or mean±SD.

Also see **Figure 2**.

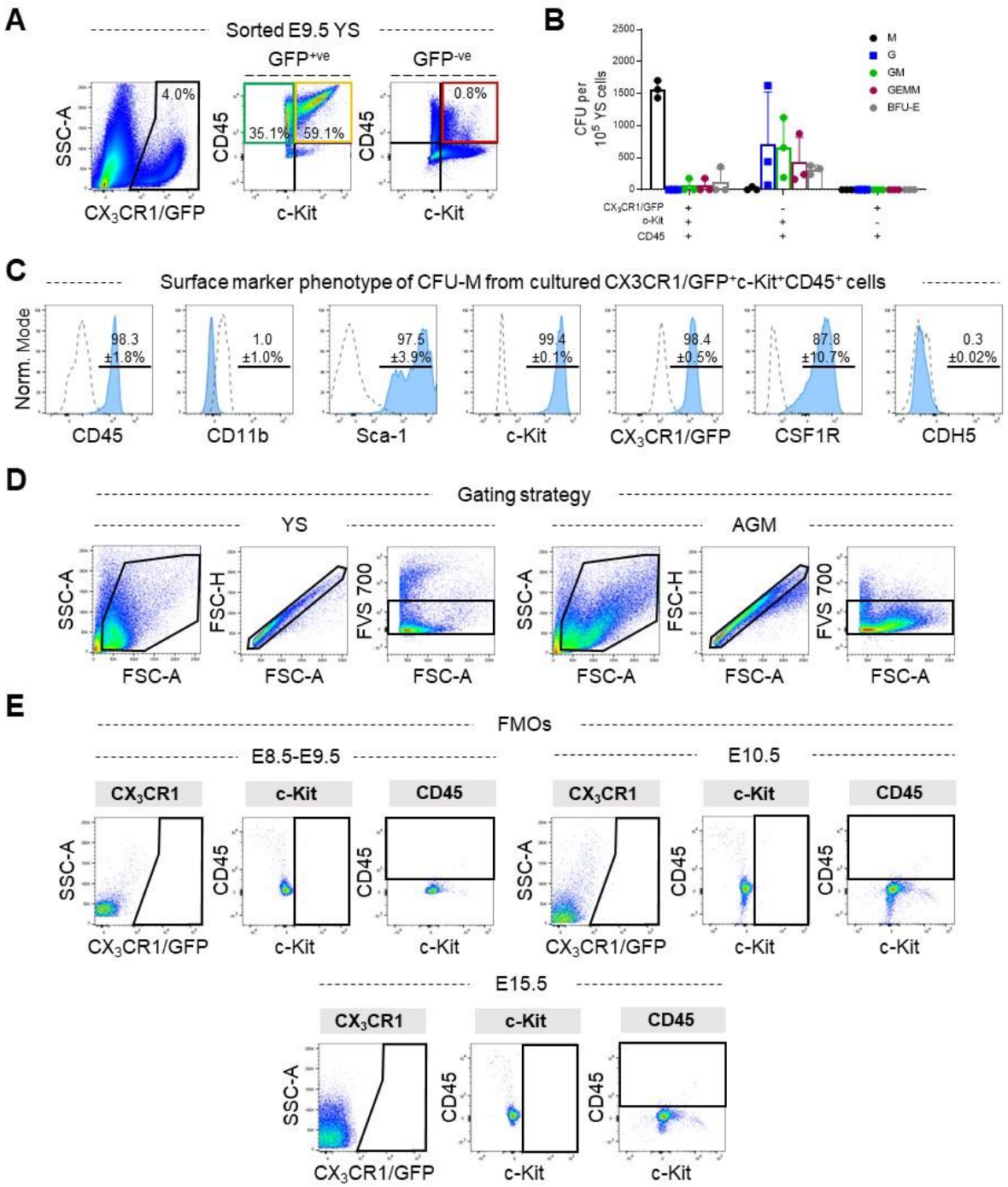

Supplemental Figure S5. Identification of CFU-M progenitors in E9.5 Yolk Sac.

(A) Gating strategy used for FACS isolation of YS cells from E9.5 *Cx3cr1*$^{GFP/+}$ embryos into CX_3CR1/GFP^+c-Kit$^+$CD45$^+$ (yellow box), CX_3CR1/GFP^+c-Kit$^-$CD45$^+$ (green box) and CX_3CR1/GFP^-c-Kit$^+$CD45$^+$ (red box) populations, used in **Figure 2G**. Percentages in quadrants are from the parent population and relate to the example shown.

(B) Yield of different colony types from the FACS-isolated populations. N=3 experiments.

Also see **Figure 2G**.

(C) Flow cytometry histograms showing surface expression of markers (blue histograms) on cells contained in CFU-M produced by sorted YS progenitors. Dotted histograms, FMO controls. N=2-4.

(D) Gating strategy used for flow cytometry of YS and AGM cells from *Cx3cr1*$^{GFP/+}$ embryos shown in **Figure 2H**.

(E) FMO controls used for flow cytometry and FACS isolation of YS and AGM cells from *Cx3cr1*$^{GFP/+}$ embryos in **Figure 2H** and **Supplemental Figure S5**.

Data summarized as mean±SD.

Also see **Figure 2**.

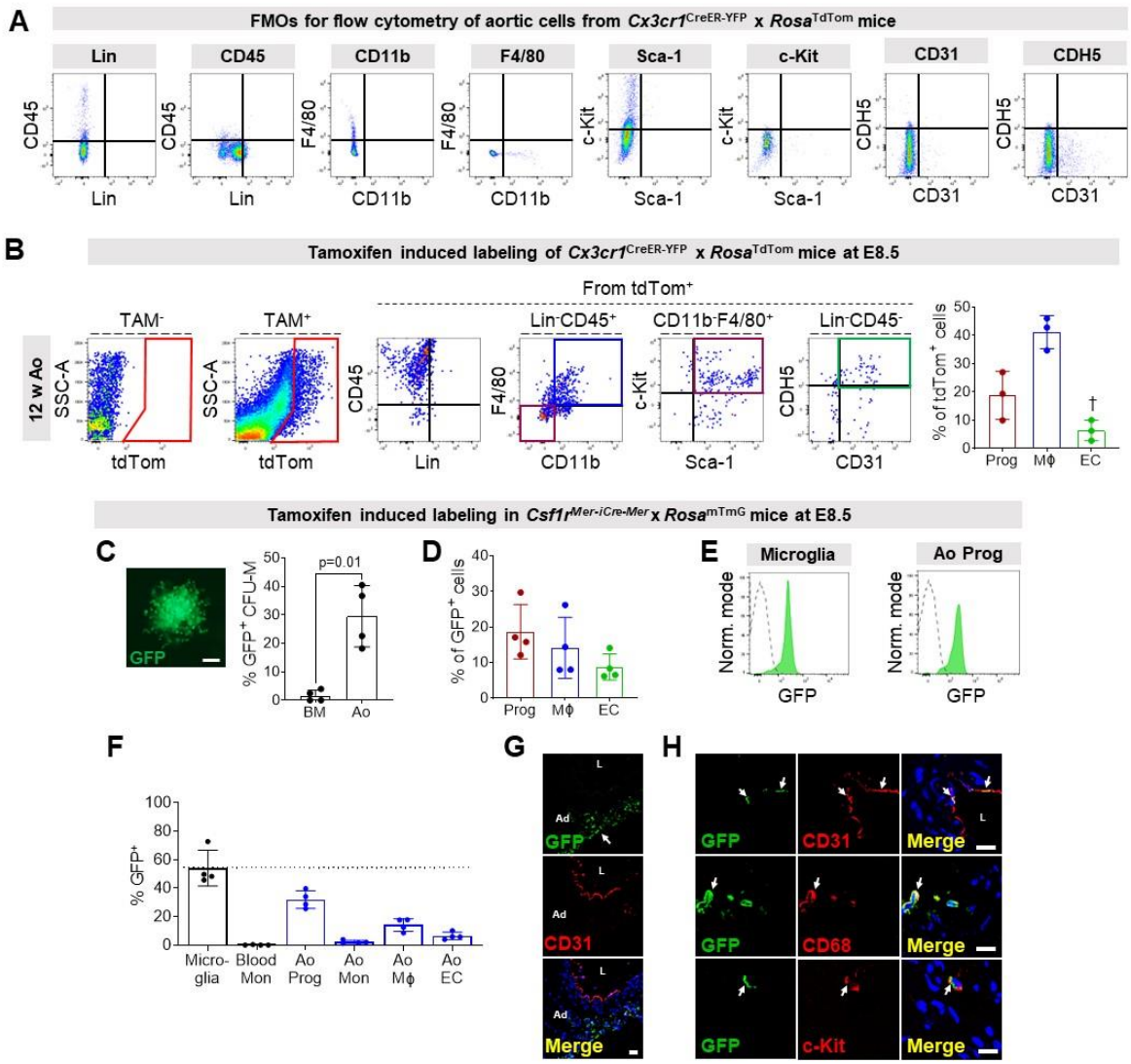

Supplemental Figure S6. Aortic CFU-M progenitors arise from CX3CR1+ and CSF1R+ cells during early embryogenesis.

(A) FMO control staining used to analyze cells from E15.5 AGM and adult aorta from *Cx3cr1*$^{\text{CreER-YFP}}$ x *Rosa*^{tdTom} mice (also see **Figure 3C, D**).

(B) Flow cytometry dot plots show composition of tdTom^{+} cells in aorta of adult *Cx3cr1*$^{\text{CreER-YFP}}$ x *Rosa*^{tdTom} mouse that had been induced with TAM *in utero* at E8.5. Gated regions correspond to macrophages (Mϕ, blue), progenitors (Prog, maroon) and endothelial cells (EC, green). tdTom expression from aorta of no tamoxifen (TAM^{-}) control also shown. Graph shows the % of tdTom^{+} cells that comprised each of these three cell populations (n=3). Repeated measures ANOVA p=0.02. Multiple comparisons test: †p<0.01 vs macrophages.

(C-H) *Csf1r*$^{\text{Mer-iCre-Mer}}$ x *Rosa*^{mTmG} mice were induced with TAM at E8.5 and analyzed at 12w.

(C) Image of GFP^{+} CFU-M from 12 w aorta. Graph shows % GFP^{+} CFU-M from aorta and BM (n=4). Paired t-test.

(D) Graph summarizes % breakdown of GFP^{+} cells in adult aorta (n=4). Repeated measures ANOVA p=0.16.

(E, F) Histograms and graph show % GFP expression in different cell populations from 12 w mice (n=4). Green histogram, sample. Dotted histogram, TAM^{-} control. Mon, monocytes.

(G, H) Confocal microscopy of immunolabeled sections of 12 w aorta shows (G) GFP^{+} cells in adventitia (Ad), with (H) magnified examples of GFP^{+} cells expressing CD31 in the intima and CD68 and c-Kit in adventitia (arrows). L, lumen.

Data summarized as mean±SD.

Scale bar, 100 μm in (A) and 20 μm in (G, H).

Also see **Figure 3**.

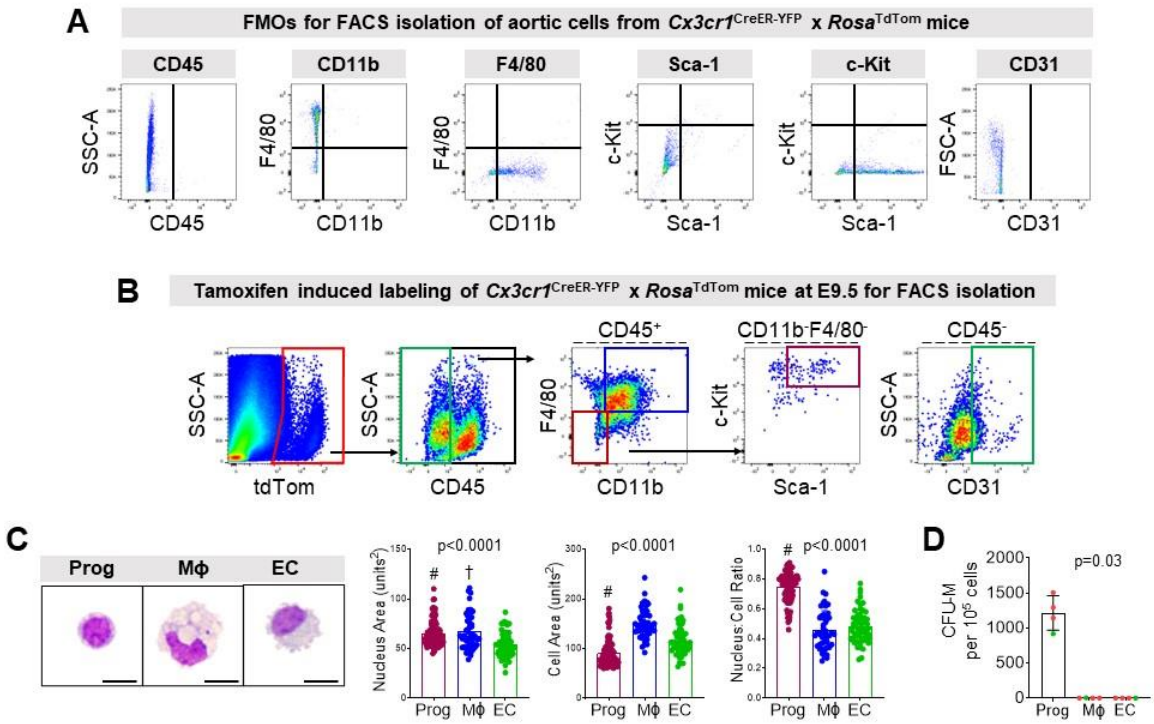

Supplemental Figure S7. Embryonic CX3CR1$^+$ cells give rise to CFU-M progenitors in postnatal aorta.

(A-D) *Cx3cr1*$^{\text{CreER-YFP}}$ x *Rosa*^{tdTom} mice were induced with TAM at E9.5 and used for FACS isolation of tdTom$^+$ aortic cells at 12 w.

(A) FMO controls used to sort aortic cells.

(B) FACS isolation of tdTom$^+$ progenitors, macrophages and endothelial cells from 12 w aorta.

(C) Wright-Giemsa staining of sorted cell populations, and graphs showing comparisons of total cell area, nucleus area and nucleus:cell area ratio (n=51-100 cells per cell type). Kruskal-Wallis tests. Multiple test comparisons: #p<0.0001 vs Mϕ and EC; †p<0.01 vs EC.

(D) CFU-M yield from tdTom$^+$ (red dots) and GFP$^+$ (green dots) progenitors, macrophages and endothelial cells isolated from adult aortas of E9.5 TAM-induced *Cx3cr1*$^{\text{CreER-YFP}}$ x *Rosa*^{tdTom} mice or E8.5 TAM-induced *Csf1r*^{MerCreMer} x *Rosa*^{mTmG} mice, respectively (total of four experiments, using six aortas each). Friedman test.

Data summarized as mean±SD.

Also see **Figure 3**.

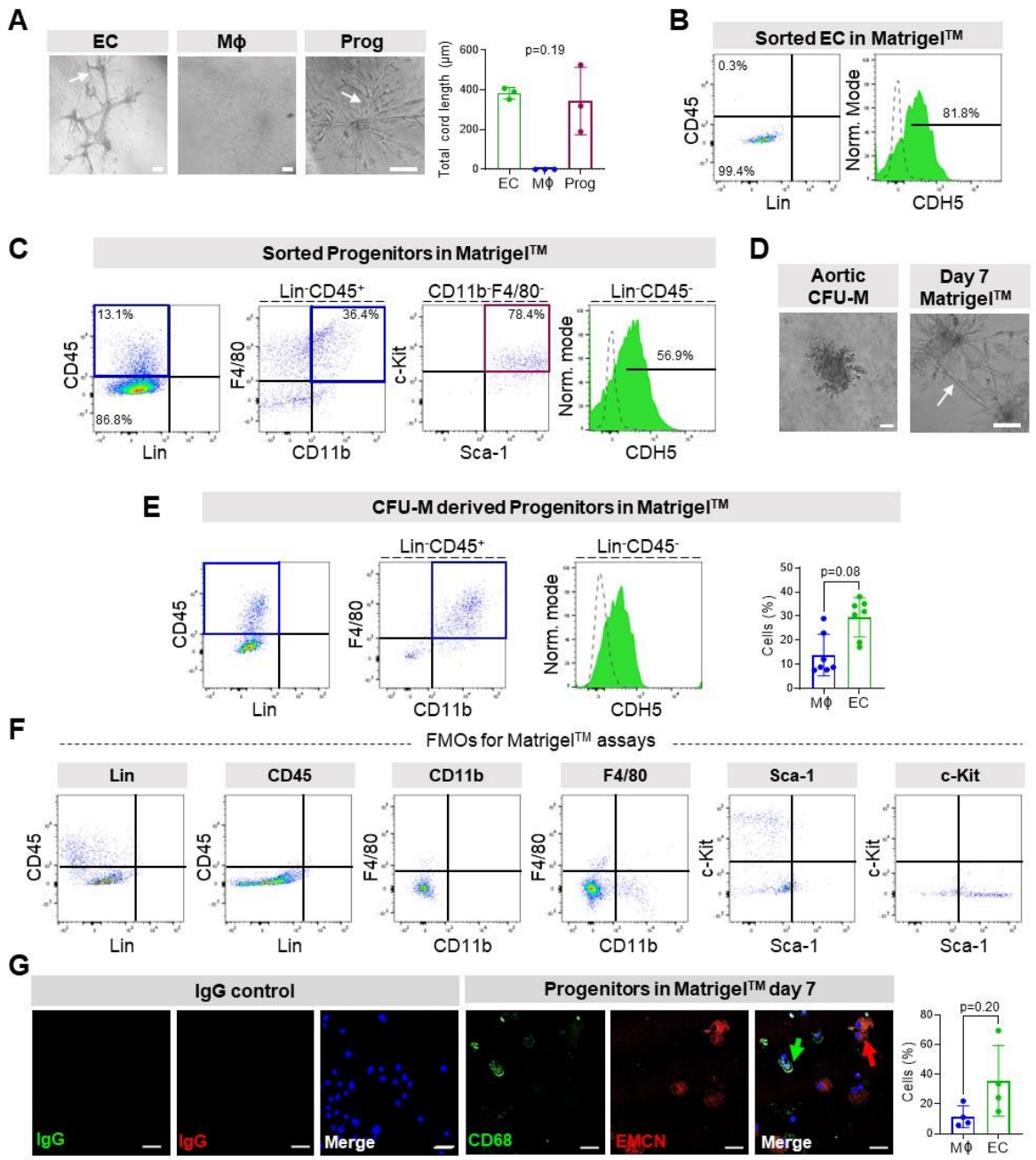

Supplemental Figure S8. Aortic CFU-M progenitors have endothelial and macrophage differentiation potential.

(A) Light microscopy images of FACS-isolated endothelial cells (EC), macrophages (Mϕ) or progenitors (Prog) from 12 w C57BL/6J aorta cultured in Matrigel™ for 7 d. Arrows indicate cords. Graph shows total cord length (three experiments, six aortas each). Friedman test.

(B, C) Flow cytometry plots and histograms show the cell types produced from culturing FACS-isolated primary aortic (B) endothelial cells and (C) progenitors in Matrigel™ (n=1

experiment using six pooled aortas). Green histogram, sample; dotted histogram, FMO control.

(D) Example of an aortic CFU-M and branching cord networks (arrow) produced from CFU-M derived progenitors in Matrigel™.

(E) Flow cytometry plots and graph show the cells produced from CFU-M progenitors cultured in Matrigel™ for 7 d (n=7 adult C57BL/6J aortas, three independent experiments). Wilcoxon signed-rank test.

(F) FMO controls for (B), (C) and (E) above.

(G) Confocal microscopy of immunolabeled cytospin preparations of cells produced by CFU-M progenitors cultured in Matrigel™ for 7 d. Cells stained with nuclear dye DAPI (blue) and immunolabeled for CD68 (green) and endomucin (EMCN; red). Graph summarizes frequency of $CD68^+$ and $EMCN^+$ cells (n=4 independent experiments). Paired *t*-test.

Data summarized as mean±SD.

Scale bar, 40 µm in (A, D) and 100 µm in (G).

Also see **Figure 4**.

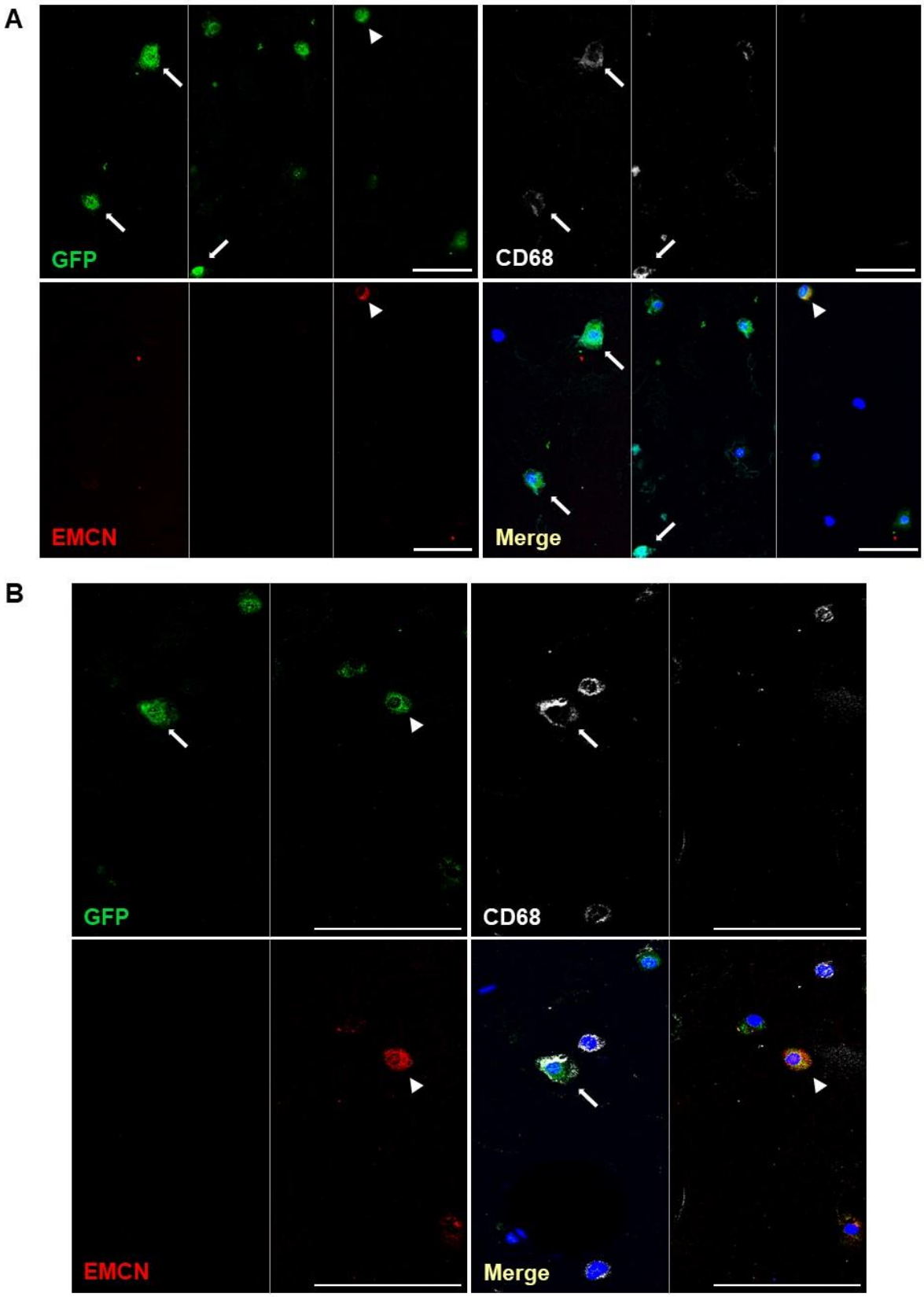

Supplemental Figure S9. Aortic CFU-M progenitors are bipotent for endothelial cells and macrophages at a single cell level.

(A, B) A single GFP^+ aortic CFU-M progenitor cell was seeded with GFP^- progenitors on

Matrigel™ in individual wells and cultured for 7 d. Cytospun preparations of resulting sprouts were immunolabeled as indicated. Confocal microscopy images of immunolabeled cells from two independent wells (A and B) show presence of GFP^+CD68^+ macrophages (arrows) and GFP^+EMCN^+ endothelial cells (arrowheads). $GFP^+CD68^-EMCN^-$ cells and GFP^-CD68^+ macrophages can also be seen. A montage of 2-3 fields of view per well is presented. White vertical lines demarcate the fields of view.

Scale bar, 100 µm.

Also see **Figure 4**.

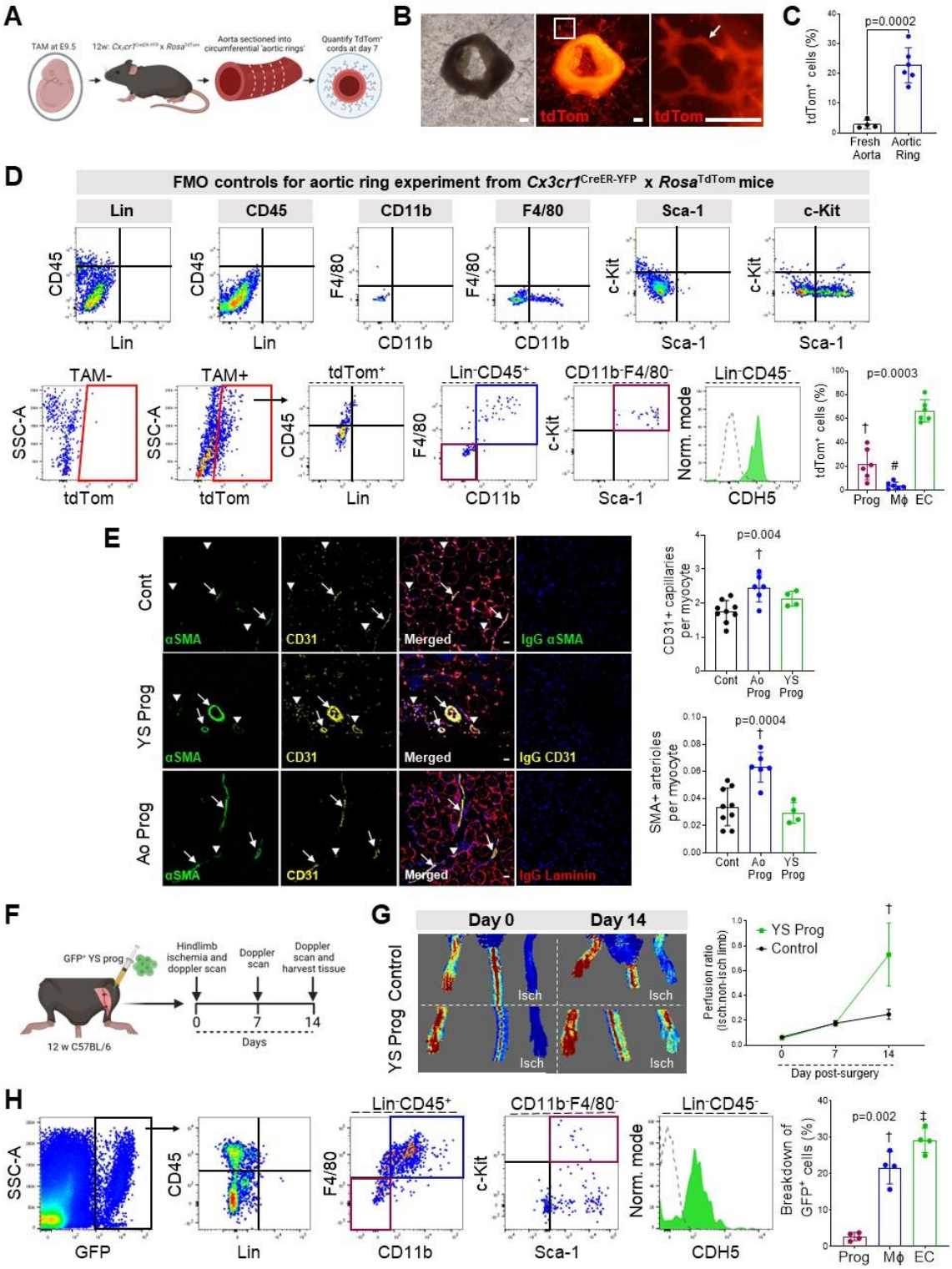

Supplemental Figure S10. Endothelial and macrophage differentiation capacity of YS-derived progenitors.

(A) Schematic for aortic ring assay performed using aortas from E9.5 TAM-induced adult *Cx3cr1*$^{\text{CreER-YFP}}$ x *Rosa*^{tdTom} mice to label embryonically derived cells tdTom^{+}.

(B) Light and fluorescence microscopy images of aortic ring show tdTom^{+} adventitial sprouting.

(C) Graph compares % tdTom^{+} expression (not normalized to microglia) in day 7 aortic ring assays with fresh digests of whole aorta. N=4-6. Unpaired t-test.

(D) Flow cytometry of aortic ring sprouting assay from 12 w *Cx3cr1*$^{\text{CreER-YFP}}$ x *Rosa*^{tdTom} mouse with TAM-induction at E9.5. Top row shows FMO controls. Bottom row shows representative sample, with gates used for macrophages (Mϕ, blue), progenitors (Prog, maroon) and endothelial cells (green histogram, EC; dotted histogram, FMO control). Also shown is the tdTom expression for the no TAM (TAM^{-}) control used in this experiment. Graph shows the composition of embryonically derived tdTom^{+} cells after aortic ring sprouting. N=6. Repeated measures ANOVA. Multiple comparison test: †p<0.01 and #p<0.0001 vs EC.

(E) Confocal microscopy of immunolabeled sections of hindlimb muscle at day 14 after ischemic surgery and receiving injections of Matrigel™ control (top) or E9.5 YS CFU-M progenitors (middle) or Aortic (Ao) CFU-M progenitors (bottom). Staining with antibodies to CD31 (yellow), αSMA (green), laminin (red) for myocytes and DAPI (blue) for nuclei. IgG negative control staining also shown. Graphs show capillary and arteriolar density. N=4-9 per group, three sections per mouse. One-way ANOVA. †p<0.01 vs control.

(F) Schematic of 1º transfer of GFP^{+} YS CFU-M progenitors into hindlimb muscle after hindlimb ischemia surgery with two-week follow-up.

(G) Laser Doppler perfusion images of mice on days 0 and 14 after ischemia and receiving cell-free control (above) or YS progenitors (below). Graph shows results of follow-up. N=4 for Prog, n=6 for control. Mixed effects two-way ANOVA: p=0.0004 for time; p=0.08 for group; p=0.02 for time x group. Multiple comparison test: †p<0.01 for Prog vs control.

(H) Flow cytometry plots and graph show cells produced by GFP^+ YS progenitors in recipient hindlimb muscle. N=4. Green histogram, sample; dotted, FMO control. Repeated measures ANOVA. Multiple comparison test: †$p<0.01$ and ‡$p<0.001$ vs Prog.

Data summarized as mean±SD.

Scale bar, 100 μm (B, E).

Also see **Figure 5**.

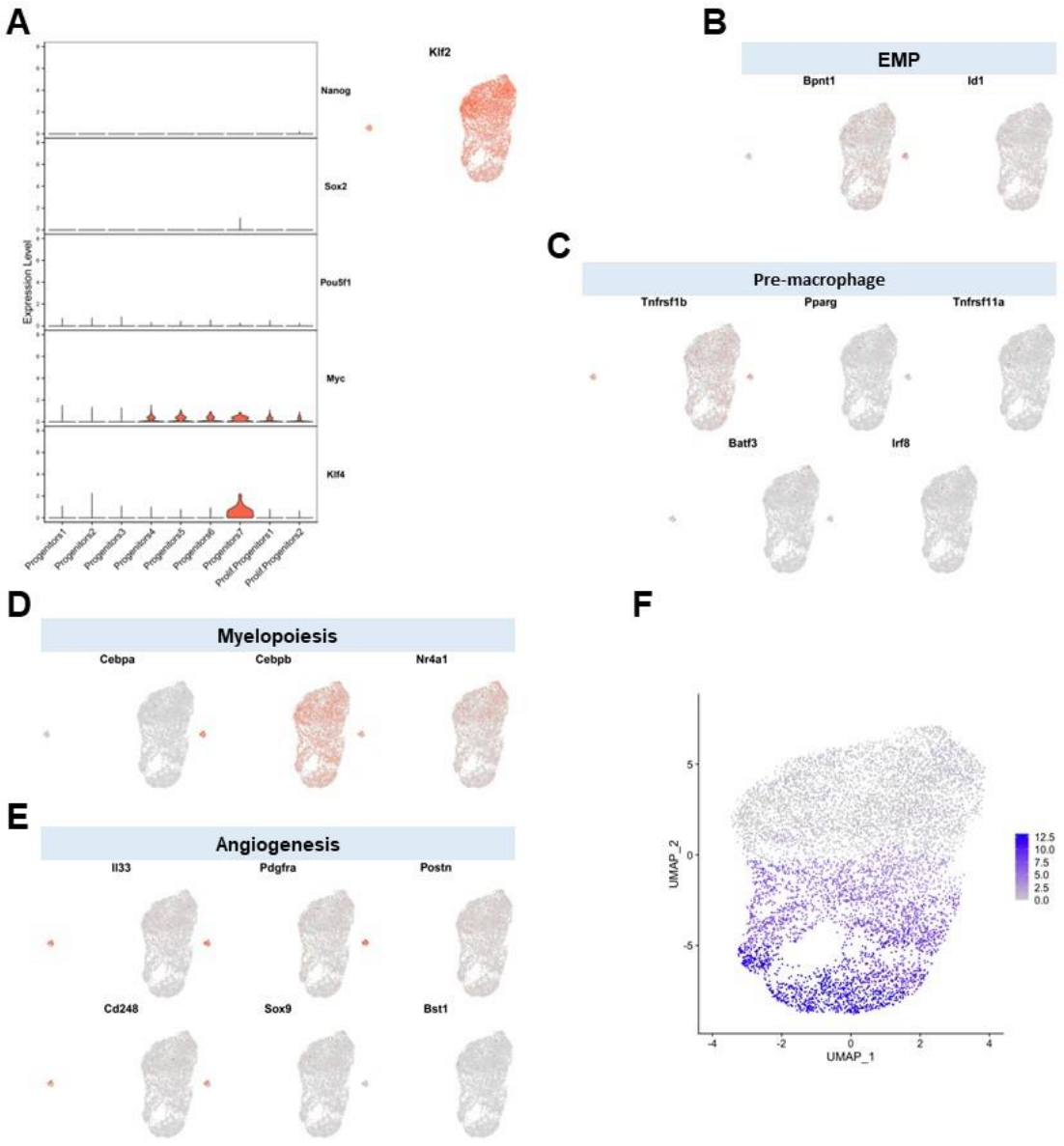

G

Cluster	Salient significantly overrepresented pathways
Prog 1	Immune system; long-term potentiation; EPO, NGF, VEGF, IL, MAPK and Notch signaling
Prog 2	Protein translation; immune system; IL and cytokine-cytokine receptor signaling
Prog 3	Immune system; Rho GTPases, MAPK, NGF, TGF-beta and TGFBR signaling
Prog 4	Protein synthesis, metabolism and targeting; mitochondrial energy production
Prog 5	Gene expression; mitotic cell cycle; mitochondrial energy production
Prog 6	Mitochondrial energy production; mitotic cell cycle, protein synthesis; adaptive immune system
Prog 7	ECM organization and degradation; ECM-cell interaction; VEGF signaling
Prolif. Prog 1	mitotic cell cycle; mitochondrial energy production; apoptosis
Prolif. Prog 2	mitotic cell cycle; mitochondrial energy production; apoptosis; immune system

Supplemental Figure S11. Aortic CFU-M progenitors exhibit a myelopoietic and vasculogenic transcriptional profile with a continuum of cell states.

Aortic CFU-M progenitors cultured from two adult C57BL/6J mice were pooled and viable cells analyzed by scRNA-seq.

(A) Violin plots illustrate cluster-wise expression of selected stem cell genes (left) and UMAP plot overlaid with expression of *Klf2* (right) showing cell specificity of expression.

(B-E) Expression levels of the indicated marker genes for B) EMPs, C) pre-macrophages, D) myelopoiesis and E) angiogenesis overlaid on the UMAP plot showing cell specificity of expression. Expression levels in A-E are shown as log normalized counts. The gray to red gradient represents low to high expression.

(F) UMAP plot showing trajectory analysis of single cells in pseudotime. Cells are colored by pseudotime. The analysis showed progression of cell states from cluster 1 at the top to proliferative clusters at the bottom. The Monocle3 algorithm identified Cluster 7 as a separate partition, thus it was not included in the analysis.

(G) The table lists the notable overrepresented pathways in the assigned cell clusters. Pathway analysis was performed using InnateDB. EPO, erythropoietin; NGF, nerve growth factor; VEGF, vascular endothelial growth factor; IL, interleukin; MAPK, mitogen activated protein kinase; TGF, transforming growth factor; TGFBR, transforming growth factor-beta receptor; ECM, extracellular matrix.

Also see **Figure 6**.